iScience

CellPress

Article

Binding of Drug-Activated CAR/Nr1i3 Alters Metabolic Regulation in the Liver

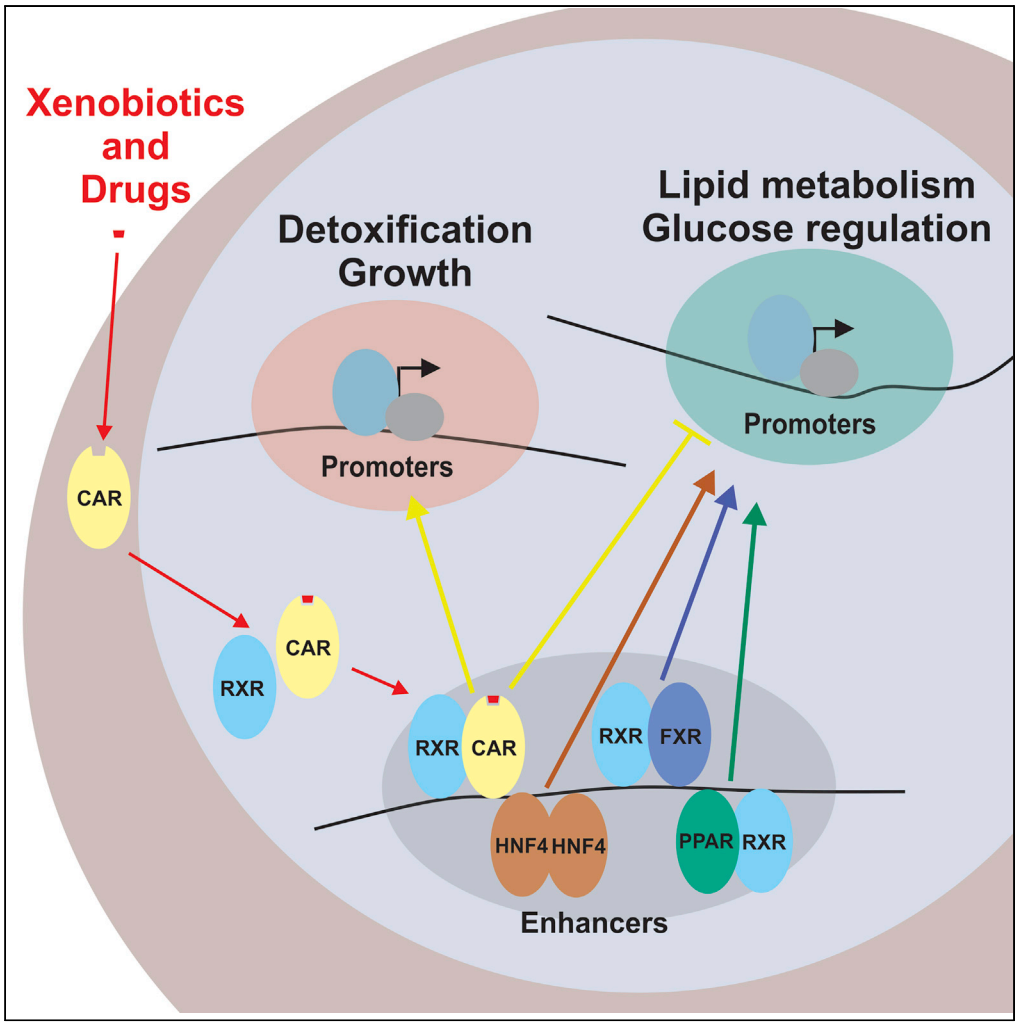

Jianmin Tian, Rebecca Marino, Carla Johnson, Joseph Locker

jlocker@pitt.edu

HIGHLIGHTS

CAR activation stimulates a massive liver transcriptional response

Target genes control drug detoxification, general metabolism, and liver growth

CAR stimulates genes through coactivation and histone acetylation

CAR inhibits genes when it shares their enhancers with other nuclear receptors

Tian et al., iScience 9, 209–228
November 30, 2018
https://doi.org/10.1016/j.isci.2018.10.018

iScience

CellPress

Article

Binding of Drug-Activated CAR/Nr1i3 Alters Metabolic Regulation in the Liver

Jianmin Tian,[1,2] Rebecca Marino,[1] Carla Johnson,[1] and Joseph Locker[1,3,*]

SUMMARY

The constitutive androstane receptor (CAR/Nr1i3) regulates detoxification of drugs and other xenobiotics by the liver. Binding of these compounds, activating ligands, causes CAR to translocate to the nucleus and stimulate genes of detoxification. However, CAR activation also changes metabolism and induces rapid liver growth. To explain this gene regulation, we characterized the genome-wide early binding of CAR; its binding partner, RXRα; and the acetylation that they induced on H4K5. CAR-linked genes showed either stimulation or inhibition and regulated lipid, carbohydrate, and energy metabolism, as well as detoxification. Stimulation of expression increased, but inhibition did not decrease, H4K5Ac. Transcriptional inhibition occurred when CAR bound with HNF4α, PPARα, or FXR on the same enhancers. Functional competition among these bound nuclear receptors normally coordinates transcriptional resources as metabolism shifts. However, binding of drug-activated CAR to the same enhancers adds a new competitor that constitutively alters the normal balance of metabolic gene regulation.

INTRODUCTION

The constitutive androstane receptor (CAR/*Nr1i3*), an important nuclear receptor (NR) transcription factor in hepatocytes, regulates genes that detoxify drugs and xenobiotics. CAR controls an unusually strong transcriptional response that also regulates liver growth and cell proliferation, promotes cancer, and alters glucose metabolism and cholesterol homeostasis (Kobayashi et al., 2015; Tian et al., 2011).

CAR-binding activators—drugs and xenobiotics—are agonist ligands that stimulate translocation to the nucleus. Following translocation, CAR heterodimerizes with RXR to bind a characteristic DNA site within transcriptional enhancers (Choi et al., 1997; Wei et al., 2000). This direct repeat 4-binding site (DR4) consists of two 6-bp half sites that bind RXR and CAR, separated by 4 bp. The so-called phenobarbital response element (PBRE) was the first CAR site to be characterized and is −2.3 kb from the transcription start of *Cyp2b10*, a gene with exceptional induction by CAR activators (Kawamoto et al., 1999). The halogenated hydrocarbon TCPOBOP (1,4-bis[2-(3,5)-dichoropyridyloxy] benzene), a specific ligand for mouse CAR, induces transcription of characteristic target genes from very low basal levels (Columbano et al., 2005; Locker et al., 2003; Tzameli et al., 2000). Moreover, the dramatic growth response to a single dose doubles the liver mass by 18 hr (Tian et al., 2011).

Several close relatives of CAR are important hepatocyte regulators with similar binding sites: homodimeric HNF4α and RXR heterodimeric partners PPARα, FXR, LXRα/β, PXR, and THRα/β. HNF4α is the central regulator of hepatocyte phenotype (Fang et al., 2012). CAR and the other RXR partners control metabolic processes within this phenotype. PPARα regulates genes of fatty acid oxidation and transport following activation by ligands such as unsaturated fatty acids, eicosanoids, and clofibrate drugs (Rakhshandehroo et al., 2007). FXR, activated by bile acids, controls cholesterol catabolism by regulating genes of bile acid transporters, apolipoproteins, and carbohydrate and amino acid metabolism (Kim and Moore, 2017). LXR—activated by oxidized cholesterol derivatives—stimulates genes of fatty acid and triglyceride synthesis and cholesterol conversion to bile acids (Boergesen et al., 2012). PXR, like CAR, is a drug and xenobiotic receptor. Ligands for CAR and PXR are generally distinct but their gene regulation overlaps (Cui and Klaassen, 2016). The thyroid hormone receptor (THR) regulates liver genes of lipid, fatty acid, and steroid metabolism (Grontved et al., 2015).

All these NRs activate transcription via their ligand-binding domains (LBDs), which directly bind p160 coactivators. As part of transcriptional activation, the p160s acetylate histones 3 and 4 at several sites, particularly histone 3 lysine 9 (H3K9) and H4K5 (Li et al., 2003; Spencer et al., 1997). In addition, the p160s bind

[1]Department of Pathology, School of Medicine, University of Pittsburgh, 200 Lothrop St, Pittsburgh, PA 15261, USA

[2]Present address: Department of Surgery, Children's Hospital of Pittsburgh, School of Medicine, University of Pittsburgh, 4401 Penn Ave, Pittsburgh, PA 15224, USA

[3]Lead Contact

*Correspondence: jlocker@pitt.edu

https://doi.org/10.1016/j.isci.2018.10.018

another coactivator, CBP, that acetylates H3K27 (Pasini et al., 2010; Tie et al., 2009). Without activating ligands, most NRs can also repress transcription through recruitment of corepressors that deacetylate histones. However, activated NRs stimulate some genes, whereas they inhibit others. This alternate type of inhibition has an important effect on phenotype, but the mechanism is poorly understood.

CAR dimerizes with RXR and binds to DNA like other NRs, but distinctive features simplify its effects and make CAR a valuable tool for examining transcriptional regulation *in vivo*. (1) Most NRs modulate activation and repression through their LBDs, but the CAR LBD has an the unusual conformation that prevents binding of corepressors. CAR is thus a pure transcriptional activator (Suino et al., 2004). (2) CAR resides in the cytoplasm unless ligand or signal transduction activates nuclear transport (Kawamoto et al., 1999). CAR-initiated transcription depends on this translocation. Hence, basal activity is very low but activation of target genes is rapid. (3) CAR lacks an N-terminal activation domain. Such domains provide a second activation mechanism for other NRs.

In this article, we present the chromatin immunoprecipitation sequencing (ChIP-seq) characterization of CAR, with parallel genome-wide characterization of RXR binding, chromatin H4K5 acetylation, and DNaseI hypersensitive sites (DHS). To correlate these dynamic modifications of chromatin with gene expression, we defined the hepatocyte transcriptome, its response to CAR activation, and the association of specific CAR binding sites to regulated genes. The analyses showed distinctive differences between gene stimulation and inhibition by CAR and suggested that inhibition was related to binding of a second NR. We therefore characterized HNF4α binding and its relationship to CAR, followed by analysis of RXR dimeric partners from published datasets. The following study of CAR thus reveals a competitive antagonism among activating NRs that controls the dynamic balance of liver metabolic regulation.

RESULTS

Validation of CAR ChIP-Seq via Candidate Gene Analysis

CAR activation in the liver transcriptionally regulates genes of detoxification and metabolism while stimulating growth and cell proliferation. The transcriptional responses could reflect direct regulation by CAR or regulation by CAR-induced factors. The responses could also be consequences of general processes like cell proliferation or of indirect mechanisms like depletion of coregulators.

To discriminate direct regulation, we carried out ChIP-seq analysis of CAR binding in liver 3 hr after treatment with TCPOBOP (Figures 1 and S1). The responses are sexually dimorphic, so analysis was simplified by an exclusive focus on young mature female mice without dietary manipulation (Ledda-Columbano et al., 2003; Waxman et al., 1985). CAR antibodies have been problematic, but our prior studies characterized a CAR-binding antibody suitable for conventional ChIP (Tian et al., 2011), and we established highly specific ChIP-seq conditions with this antibody (see Transparent Methods). The specificity is exemplified by the demonstration of 3 CAR-binding enhancers in the region upstream of *Cyp2b10* (Figures 1A and 1B), including the PBRE within CAR peak 3 (Kawamoto et al., 1999). The binding coincides with strong transcriptional stimulation (Figure 1C).

CAR detection was complemented by analysis of RXRα, promoter marker H3K4Me3, DNaseI hypersensitivity (DHS), enhancer marker H4K5Ac, and RNA sequencing (RNA-seq). The enhancer marker H4K5Ac was chosen because it directly reflects transcriptional activation by NR (Li et al., 2003; Spencer et al., 1997) and we validated its application by comparing with more common markers of enhancer activation, H3K9Ac and H3K27Ac (Figure S2). For all 3, CAR bound to "valleys" within a field of acetylation. H4K5Ac provided the strongest enhancer detection, the highest discrimination between promoters and enhancers, and greatest changes following TCPOBOP treatment. The relative sensitivity of H4K5Ac detection is exemplified by the changes surrounding CAR enhancer peak 1 (Figure S2B). Because it marked the largest number of enhancer regions, H4K5Ac also provided valuable discrimination of specific and non-specific binding peaks.

Many studies have used DHS to mark enhancers and their activation. However, most enhancer regions of CAR-regulated genes showed only moderate levels of DHS, which was much more prominent at promoters of unrelated genes (Figure S2). Compilation of sequence tags around CAR showed an almost identical distribution of RXR binding in the center of DHS regions. CAR, RXR, and DHS were surrounded by regions of H4K5Ac, which, however, was centrally depleted (Figure 1D). Because of their sensitivity and

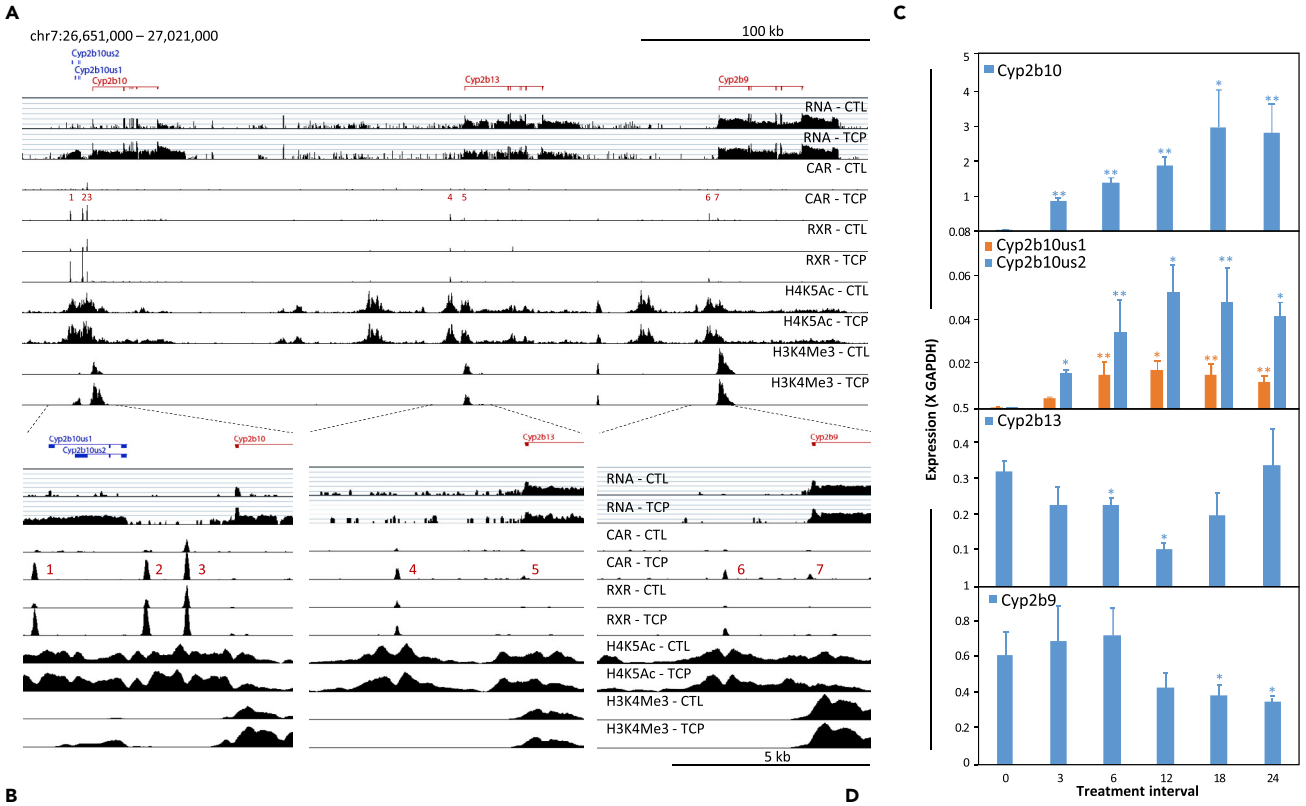

B

Peak	Gene	dTSS	CAR		RXR	CAR/RXR	H4K5Ac
			TCP/CTL	*p (-log10)*	*TCP/CTL*	*TCP*	*TCP/CTL*
1	Cyp2b10	-9697	11.5	33.775	6.4	1.2	1.3
2	Cyp2b10	-4367	8.6	32.643	6.0	0.9	1.2
3	Cyp2b10	-2317	3.6	43.333	2.1	1.4	1.0
4	Cyp2b13	-6104	5.1	18.498	1.6	2.2	1.0
5	Cyp2b13	-24	1.1	8.345	0.0	17.7	1.2
6	Cyp2b9	-4128	4.3	19.771	3.8	2.0	1.0
7	Cyp2b9	-28	3.1	9.915	0.0	44.2	0.9

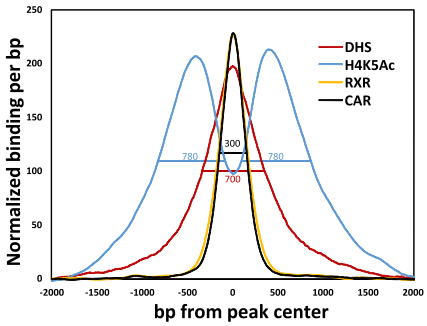

Figure 1. Correlation of CAR Binding in the *Cyp2b10-Cyp2b13-Cyp2b9* Gene Cluster

Discrete CAR peaks were induced upstream of each gene within regions of H4K5Ac, most at sites that previously bound RXR.

(A) Genomic distribution of transcripts, CAR, RXR, H4K5Ac, and H3K4Me3. TCP, TCPOBOP for 3 hr; CTL, control. ChIP-seq and RNA-seq were visualized with GenPlay (Lajugie and Bouhassira, 2011) using linear and $\log_{10}$ scales, respectively. Scale bars: above, 100 kb, below, 5 kb.

(B) Parameters of CAR binding. For the peaks identified in (A), the columns show distance to the nearest promoter (dTSS); stimulation ratios of CAR, RXR, and H4K5Ac (all as TCP/CTL); p values of CAR peaks; and ratios of CAR to RXR binding in TCPOBOP-treated liver.

(C) qRT-PCR analysis of transcripts. Plots show mean and SD from at least 3 livers at each time. *$p < 0.5$, **$p < 0.01$.

(D) General relationship of CAR, RXR, DHS, and H4K5Ac binding. Distributions of aligned tags were calculated from the complete set of CAR peaks. Patterns were normalized for display and show the peak width at half height.

complementary relationships, we integrated analysis of NR and H4K5Ac. DHS was analyzed separately, and an additional chromatin modification, H3K4Me3, was used only as a marker of active promoters.

TCPOBOP treatment strongly stimulated CAR binding of the PBRE (peak 3) and two novel enhancers (peaks 1 and 2) near the *Cyp2b10* promoter (Figures 1A and 1B). RXR binding and acetylation in control liver indicated that these enhancers were active before CAR binding. Treatment also stimulated transcription of an upstream gene (*Cyp2b10us*, with 2 spliced isoforms), 5.2 kb from *Cyp2b10* (cloned by RACE; GenBank: MF399062, MF399063). *Cyp2b10us* is a long non-coding RNA without significant open reading frames and

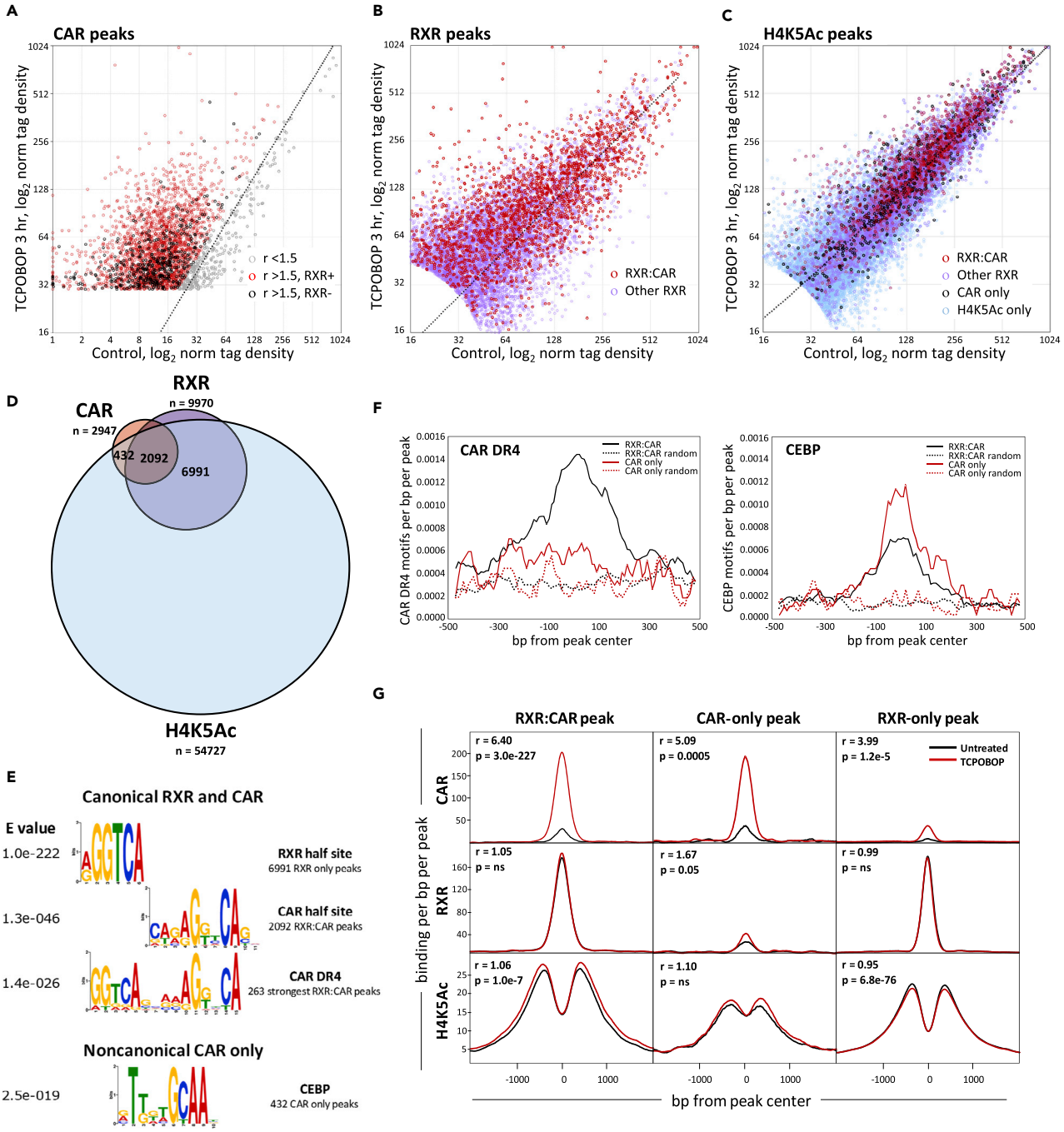

Figure 2. Characterization of CAR Peaks

(A) The CAR peak set. The plot discriminates H4K5Ac^{+} RXR:CAR (red), CAR-only (black), and peaks excluded because the stimulation ratio was <1.5 (gray).

(B) The RXR peak set. The plot discriminates H4K5Ac^{+} RXR:CAR (red) and other RXR peaks (blue).

(C) The H4K5Ac narrow peak set. The plot discriminates overlapping—CAR + RXR (red), CAR only (black), or RXR only (purple)—and non-overlapping (blue) subsets.

(D) Overlap of CAR, RXR, and H4K5Ac peak sets.

(E) MEME-ChIP analysis showing prominent motifs calculated *de novo* from peak subsets.

(F) Distribution of CAR DR4 and CEBP motifs on RXR:CAR and CAR-only peak subsets. Control analysis used random sequences matched for length and chromosome location.

Figure 2. *Continued*

(G) Tag density histograms and statistical analysis showing effects of TCPOBOP treatment. Sets from (D) were RXR:CAR (n = 2,092), CAR-only (n = 432), and RXR-only (n = 6,991) peaks. Stimulation ratios were calculated from histogram peak summits (CAR and RXR) or the average of two summits (H4K5Ac). Statistical analysis derived from parallel analysis of tag density on individual peaks. For H4K5Ac, tag density was calculated from a window of −825 to +825 bp around the peak center. p values were calculated using paired t tests that compared the distributions of control and treated values.

lacks homology with the Cyp2b10 transcription unit. Of note, the induction of *Cyp2b10us* demonstrates that CAR-binding enhancers link to regulation of multiple genes.

Two closely related P450 genes, *Cyp2b13* and *Cyp2b9*, are 164 and 276 kb, respectively, from *Cyp2b10*. Each gene had 2 CAR peaks near the promoter, one with and one without RXR. CAR strongly induced *Cyp2b10* and *Cyp2b10us*, whereas *Cyp2b13* and *Cyp2b9* were both downregulated but with different time courses (Figure 1C). Induced CAR binding therefore associates with both increased and decreased transcription from different target genes.

Gadd45b, another strongly induced candidate gene (Tian et al., 2011), associated with more distant CAR-binding enhancers within adjacent *Gng7*, 29–60 kb from the *Gadd45b* promoter (Figure S1A). In addition to strong CAR-binding peaks, TCPOBOP also induced weak but significant CAR binding to other RXR sites within *Gng7*, a change noted throughout the genome. Upregulation of another candidate target, *Myc*, associated with induced CAR peaks at +343 and +361 kb (Figure S1B), whereas the intervening gene *Pvt1* showed downregulation. Direct CAR regulation of *Myc* is possible, since even more distant enhancers control this gene (Uslu et al., 2014) and other regulated genes are far more distant from the induced CAR peaks. Because of the *Myc* relationship, we used 400 kb as the cutoff for linking CAR peaks to regulated genes.

Characterization of a Specific CAR Peak Set

Candidate analysis detected induced CAR binding near numerous regulated genes and validated the ChIP-seq analysis. We therefore compiled a genome-wide CAR peak set (Feng et al., 2012). Although significant peaks associated with virtually all known CAR targets, they were overshadowed by thousands of much stronger peaks that did not link to regulated genes. These latter peaks were restricted to a small fraction of the genome where similar peaks were detected with control antibodies. We therefore defined 624 genomic segments that could not be analyzed by ChIP-seq (see Transparent Methods and Table S1). These segments—totaling 17.4 mb, 0.7% of the mm9 genome including 62 genes (Table S2)—were filtered before analysis of the remaining 2,553 mb.

Analysis of the remaining genome with MACS2 software (Feng et al., 2012) generated a set of 37,000 CAR peaks with p value < 0.001 (Figures 2A and S3A). Such large peak sets are common, but the number of peaks presents a significant barrier to correlation with specific gene regulation, so secondary cutoffs were derived from binding strength. Elimination of the bottom 2% of the range of peak strength reduced the peak number to 5,400, whereas elimination of 3% left only 3,500 peaks. RXR (9,970 peaks) and H4K5Ac (54,727 peaks) sets (Figures 2B, 2C, S3B, and S3C) were similarly restricted to the top 97% of the range of binding strength. The ratio of top 97% to top 98% peaks was 0.65 for CAR and 0.73 for RXR. The CAR ratio is a little smaller but does not extrapolate to a big difference between expected and observed binding sites.

True CAR peaks have another defining property, binding induced by TCPOBOP treatment. A cutoff ratio of 1.5 (treated/control) excluded nonstimulated peaks, and further reduced the peak set to ~3,000. As a final discriminator, overlap with H4K5Ac-positive regions selected ~2,500 peaks within regions of active transcriptional regulation (Figure 2D).

CAR peaks fell into 2 classes, RXR:CAR and CAR-only peaks. *De novo* analysis with MEME-ChIP software (Bailey et al., 2015) showed that the RXR:CAR and CAR-only sites were different (Figure 2E). The complete RXR:CAR peak set generated an NR-like *CAR half-site motif*, but a smaller set—263 peaks that represented the top 90% of the binding strength range—generated a complete *CAR-DR4 motif* in which the second repeat was nearly identical to the *CAR half-site motif*. Moreover, an *RXR half-site motif*, derived from RXR-only peaks, was similar to the first repeat of the DR4 motif. Scanning with the FIMO program (Bailey et al., 2015) then detected matches (p < 0.001) to the CAR DR4 motif in 1,936 of the RXR:CAR peaks, averaging 1.7 motifs per peak.

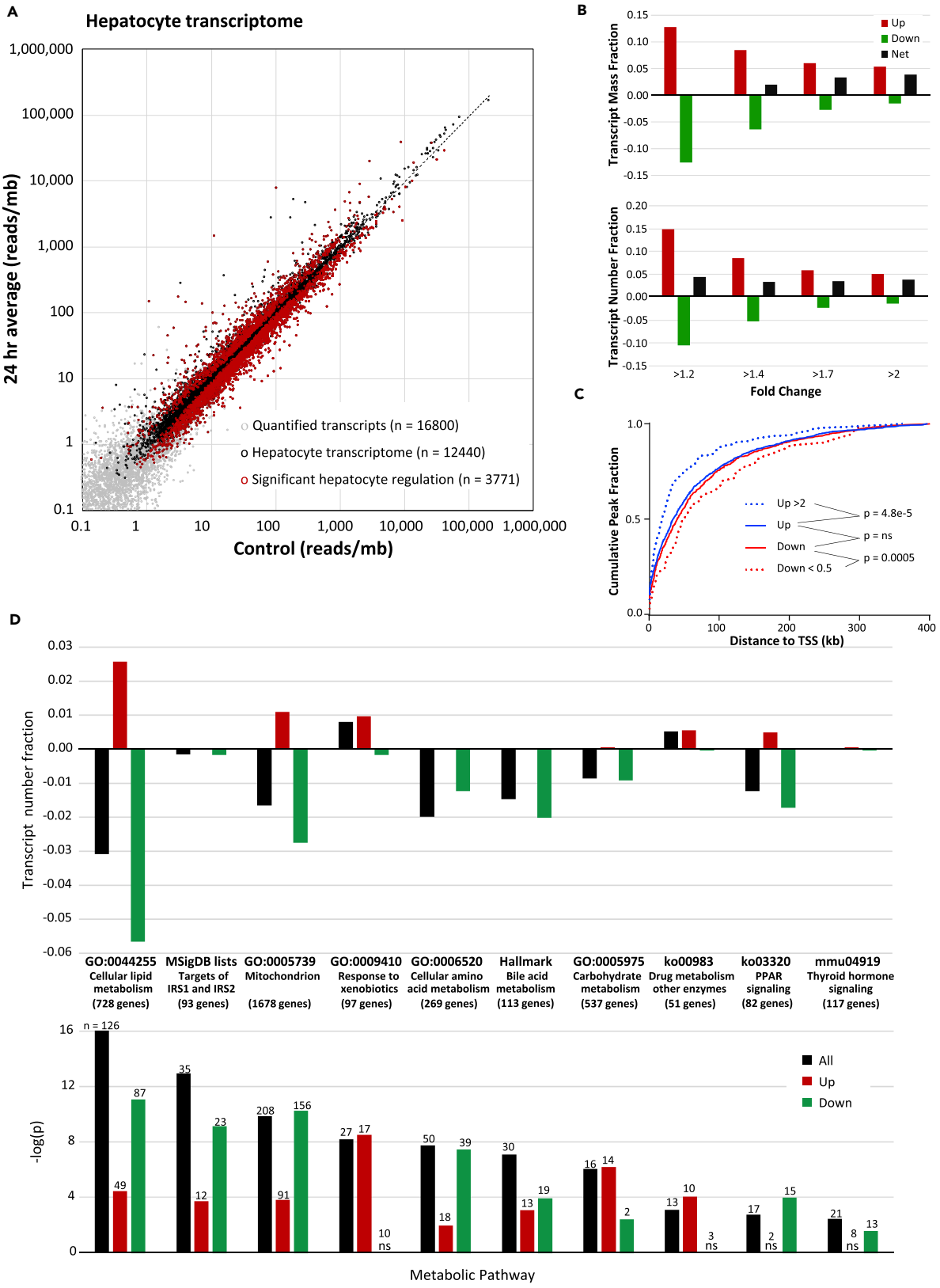
A
Hepatocyte transcriptome
24 hr average (reads/mb)
Control (reads/mb)
Quantified transcripts (n = 16800)
Hepatocyte transcriptome (n = 12440)
Significant hepatocyte regulation (n = 3771)
B
Transcript Mass Fraction
Transcript Number Fraction
Up
Down
Net
Fold Change
C
Cumulative Peak Fraction
Distance to TSS (kb)
Up >2
Up
Down
Down < 0.5
p = 4.8e-5
p = ns
p = 0.0005
D
Transcript number fraction
GO:0044255 Cellular lipid metabolism (728 genes)
MSigDB lists Targets of IRS1 and IRS2 (93 genes)
GO:0005739 Mitochondrion (1678 genes)
GO:0009410 Response to xenobiotics (97 genes)
GO:0006520 Cellular amino acid metabolism (269 genes)
Hallmark Bile acid metabolism (113 genes)
GO:0005975 Carbohydrate metabolism (537 genes)
ko00983 Drug metabolism other enzymes (51 genes)
ko03320 PPAR signaling (82 genes)
mmu04919 Thyroid hormone signaling (117 genes)
-log(p)
All
Up
Down
Metabolic Pathway

Figure 3. Correlation of CAR Peaks with Transcriptional Regulation

(A) RNA-seq analysis. The hepatocyte transcriptome was defined from transcripts enriched in isolated hepatocytes compared to whole liver. For each gene, 24-hr average regulation was calculated using RNA-seq values from 0, 3, 6, 12, 18, and 24 hr after treatment. Statistical significance was calculated with paired t tests that compared the time series for each transcript with control *Ppia* mRNA. Plotted values had a false discovery rate <0.05. See Table S3.

(B) Changes in transcript mass and number fraction. Analysis compared 24-hr average stimulation, inhibition, and net change as mass fraction (reads/gene) (B) or number fraction (reads/kb/gene) at different stimulation/inhibition ratios, each calculated as $\sum(t-c)/\sum(t)$, where t and c are treated and control values, respectively.

(C) Cumulative RXR:CAR distances to the TSS. Peaks were limited to 400 kb from the transcriptiion start site (TSS). Regulated genes, >1.2-fold change of 24-hr average expression; strongly expressed genes, >2-fold change. p values were calculated from non-paired t tests comparing the distributions.

(D) Correlations of regulated CAR-linked genes to selected ontology profiles. Upper panel, transcript number fractions; lower panel, p values and the number of correlating genes.

MEME-ChIP analysis of the CAR-only peak set did not derive an NR half-site but instead generated a CEBP motif (Figure 2E). The distribution of CEBP motifs showed central localization in both RXR:CAR and CAR-only sets with a much more significant correlation to the latter (Figure 2F). In contrast, DR4 motifs showed central localization only in RXR:CAR peaks. MEME analysis also derived FOXA motifs from RXR:CAR peaks (E = 1.9e-10), but positional analysis did not show the central localization that would indicate a close association with CAR (not illustrated).

We then compared CAR, RXR, and H4K5Ac in 3 peak sets: RXR:CAR, CAR-only, and RXR-only peaks (Figure 2G). Stimulation of CAR binding was clear in both RXR:CAR and CAR-only sets. Binding of RXR to RXR:CAR sites increased only 5%, confirming that RXR previously bound as a heterodimer to different partners, or as a homodimer, before treatment. Moreover, the moderate increase of H4K5Ac indicated that induced CAR bound predominantly to previously active enhancers.

Competition for limiting RXR is often invoked as a mechanism for transcriptional downregulation, but the binding of RXR to non-CAR sites was unchanged, ruling out this mechanism. However, the net 5% reduction of H4K5Ac on RXR-only sites was moderate but highly significant. This finding suggested an alternate inhibitory mechanism in which new CAR binding competed for H4K5-acetylating cofactors.

Relating CAR Binding to Gene Expression

The next studies related the 2,100 RXR:CAR and 400 CAR-only peaks to TCPOBOP-regulated genes. From the 24,000 unique genes in the mm9 Refseq annotation, RNA-seq libraries characterized a 12,000-gene hepatocyte transcriptome and sequential changes through the beginning of S phase at 24 hr (Figure 3A, Table S3). We began by correlating CAR binding with gene expression at 3 hr and found this time interval adequate to study most upregulation, but not downregulation. The variety of sequential regulatory patterns made the problem complex because no single time point was adequate to compare global gene regulation with CAR binding. Separate analysis of multiple time points, however, would have required a prohibitive number of replicate RNA-seq libraries and divided the peaks into small correlations. We therefore used the entire time series to determine the average expression over 24 hr, a normalized hourly value calculated from expression at 0, 3, 6, 12, 18, and 24 hr after TCPOBOP treatment, and used these inclusive *24-hr average* values for most correlations.

The analysis exploited the quantitative features of RNA-seq to integrate global changes in the transcriptome with individual genes and pathways. Total transcriptional changes were summed from the individual transcript changes in Table S3 (Figure 3B). A comparison of stimulation/inhibition ratios demonstrated that net *24-hr average* transcriptional changes of RNA mass (reads/gene) were balanced when cut off at a 1.2-fold ratio, suggesting a constant level of transcriptional elongation. In contrast, transcript number (reads/gene/kb) showed a 5% net increase of transcriptional initiation that presumably reflected the synthetic requirements of massive liver growth. With this moderate 1.2-fold cutoff, 97% of CAR peaks linked to regulated genes. In contrast, a 2-fold cutoff restricted analysis to the most prominent gene regulations associated with CAR, but linked only 37% of the binding peaks. A 1.2-fold change in gene expression may seem to be a small effect, but can actually reflect a very large increase in transcriptional initiation if the gene is strongly expressed (see Table S3). Moreover, changes of this magnitude for serum proteins, the high-abundance products of the liver transcriptome, have important biological effects.

The vast majority of CAR peaks were in distant regulatory elements within 400 kb of regulated genes (Figures 3C). The median peak-promoter distances for up- and downregulated genes were similar, 34 and

40 kb, respectively. However, for 2-fold regulation, median peak locations were significantly closer to upregulated (18 kb) and farther from downregulated genes (50 kb).

To assess the biological significance of CAR peak-associated gene expression, functional enrichment analysis (Heinz et al., 2010) compared gene number and statistical significance to ~5,000 profiles (Figure 3D). We also quantified the changes in transcript number for each response. The expected correlations of upregulated genes to xenobiotic and drug metabolism were clear and significant. Surprisingly, the correlations to lipid metabolism, the insulin-responsive IRS signal transduction pathway, and mitochondrial genes had higher statistical significance and accounted for larger changes in net transcription. In addition, downregulation dominated the nonxenobiotic responses. CAR induction therefore significantly reprioritized metabolic gene expression in addition to stimulating xenobiotic metabolism.

Functional Correlation of CAR Binding with Gene Regulation

Correlation by distance associated CAR-binding elements with 6,400 regulated genes. To examine mechanisms, however, we simplified the relationships to the two regulated genes closest to each CAR-binding peak, a set of ~2,500 genes (Figure 4A, Table S4), which accounted for ~60% of the total transcriptional change. Significantly, both closer and farther genes in the pairs contributed substantial regulation (Figure 4B).

In early studies with the full RXR:CAR peak set, correlation of chromatin changes with gene expression gave biphasic curves, an upward region of positive correlation for increased expression and a flat region of noncorrelation for decreased expression. To resolve these discordant effects, we defined 4 peak subsets with unambiguous relationships to up- or downregulation (Figure 4C). The subsets consisted of peaks associated only with a single regulated gene within 400 kb (*single up*, n = 94; *single down*, n = 179) or with 2 genes within 400 kb that had parallel regulation (*dual up*, n = 282; *dual down*, n = 572). The remaining peaks had an ambiguous relationship to gene expression, since they associated with oppositely regulated genes (*dual opposite*, defined by relative distance of the regulated genes as *up down*, n = 257; or *down up*, n = 214). The inclusive subsets together comprised 80% of all induced RXR:CAR peaks. The main reason for exclusion was when one of the linked genes only showed a transient expression change at 3 hr.

Analysis of H4K5Ac in subsets revealed a clear difference between up- and downregulation (Figure 4C). The former had increased acetylation, the expected effect of an activating NR. The latter, however, showed little change, not the histone deacetylation expected for true repression. The *dual opposite* pairs had intermediate changes dominated by regulation of the closer gene. A general comparison showed highly significant differences between up- and downregulation across the different subsets (Figure 4D).

Detailed characterization of peak subsets and linked gene expression is presented in Figure S4. Transcript number changes, CAR pileup, and CAR-binding stimulation demonstrated overall similarity of the subsets, which validated their use in our analysis. Subset expression ratios also confirmed differences between up- and downregulation (Figure S4A). Upregulation was faster and sustained, since 3- and 24-hr average median expression ratios were similar. Downregulation was delayed—median expression ratios were 0.91–0.94 at 3 hr and 0.66–0.68 in the 24-hr average. The 3-hr ratio medians were of particular interest, because even though the effects were small, they still confirmed that downregulation started soon after CAR binding. The delay most likely represents slow turnover of mRNA following inhibition by CAR. Subset comparisons also confirmed that downregulation generally occurred over a greater distance than upregulation (Figures 3C and S4E).

Parallel analysis of DHS showed differential changes in the CAR-binding peak center (Figure S5). Upregulation caused slight decrease, not the expected increase in DHS, whereas peaks of downregulated genes showed a greater but still moderate decrease. The decreases probably reflect local remodeling by altered binding of transcription factors and cofactors. The consistent differences in H4K5Ac and DHS changes confirm that up- and downregulation occur by different mechanisms rather than reciprocal changes in a single process, but neither change explains the cause of downregulation.

Regulation by CAR-Only Sites

The use of peak subsets also enabled characterization of gene regulation by CAR-only sites (Figure S6). Many CAR-only peaks regulated the same genes as RXR:CAR peaks (Table S4). However, we established

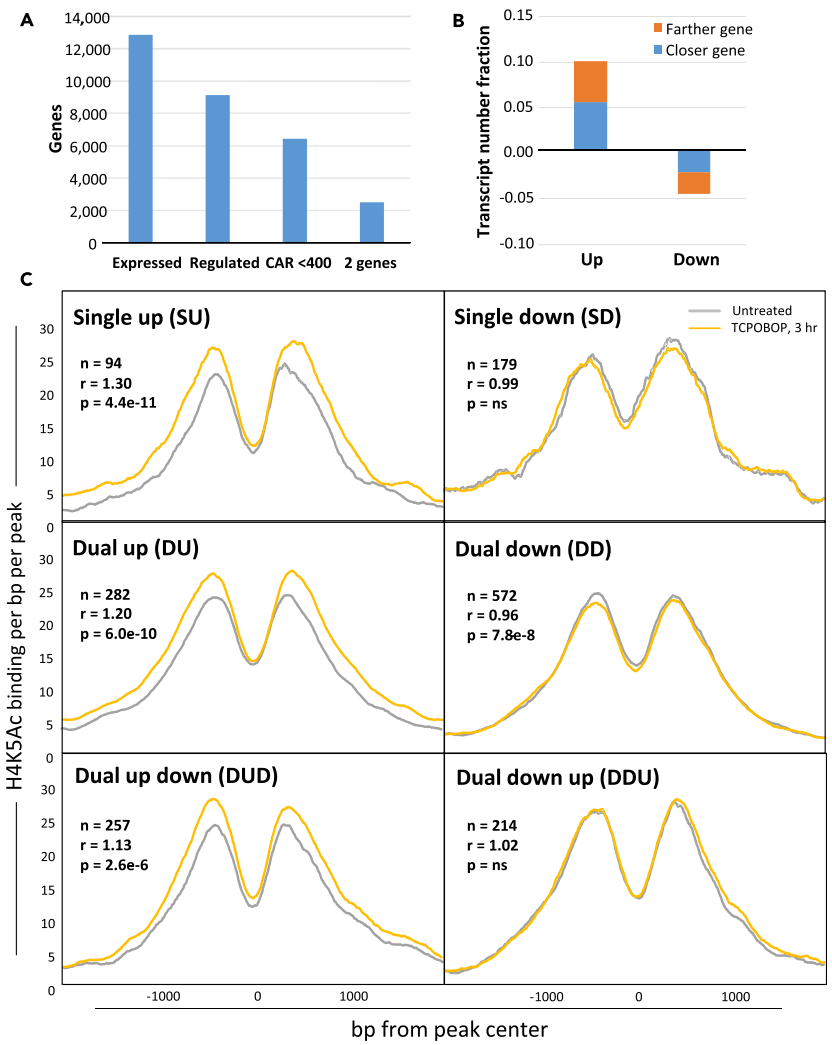

D

Comparison of stimulation ratios (p values)

Peak Sets	DU	SU	DUD	DD	SD	DDU
DU	-	0.0024	NS	1.20e-10	0.0076	0.0022
SU	0.0024	-	NS	2.24e-08	0.0019	1.10e-06
DUD	NS	NS	-	2.80e-06	0.0053	0.0007
DD	1.20e-10	2.24e-08	2.80e-06	-	NS	NS
SD	0.0076	0.0019	0.0053	NS	-	NS
DDU	0.0022	1.10e-06	0.0007	NS	NS	-

Figure 4. Refinement of the Relationship of CAR Peaks to Regulated Genes

(A) Simplification of transcriptome analysis. All groups represent expression of 24,000 *mm9* transcripts with unique Refseq gene annotations. *Enriched*, hepatocyte-enriched compared to whole liver, >0.1 transcript per cell; *Regulated*, >20% 24-hr average change after treatment with TCPOBOP; *CAR < 400 kb*, regulated genes within 400 kb of an induced CAR peak; *2 genes*, the two closest regulated genes to each CAR peak.

(B) Contributions of the 2 closest genes to regulation. Number fractions were calculated as in Figure 3B.

(C) Histogram analysis of H4K5Ac in defined peak gene subsets. H4K5Ac increased in subsets associated with upregulation but showed little change in genes associated with downregulation. *r*, ratio of treated/control peak summits; p, paired t test comparing control and treated H4K5Ac values of individual peaks, as in Figure 2G.

(D) H4K5Ac correlations among peak sets. Sets of individual peak ratios were compared using unpaired t tests.

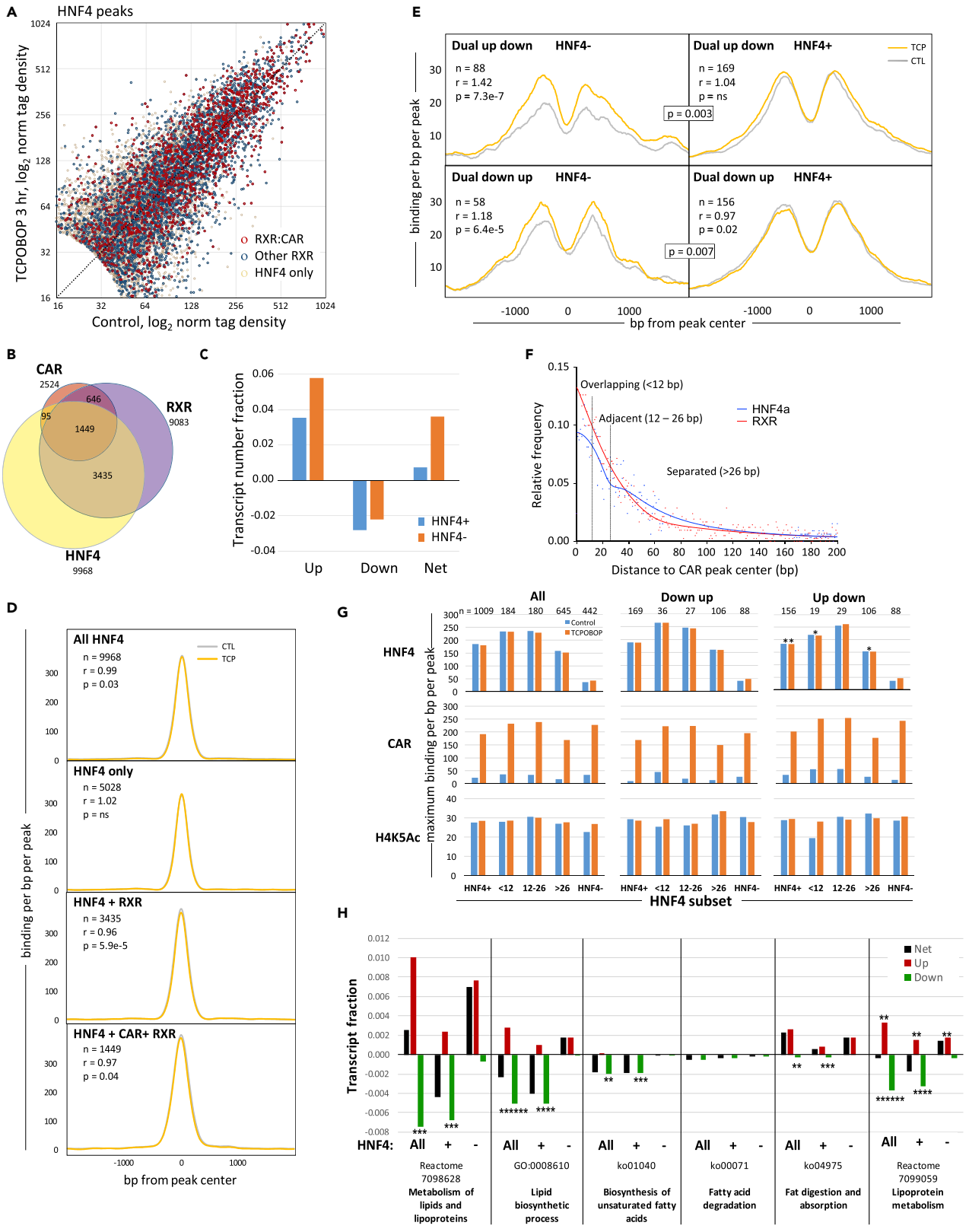
A
HNF4 peaks
TCPOBOP 3 hr, log2 norm tag density
Control, log2 norm tag density
RXR:CAR
Other RXR
HNF4 only
B
CAR
2524
646
95
1449
RXR
9083
3435
HNF4
9968
C
Transcript number fraction
HNF4+
HNF4-
Up
Down
Net
D
All HNF4
n = 9968
r = 0.99
p = 0.03
HNF4 only
n = 5028
r = 1.02
p = ns
HNF4 + RXR
n = 3435
r = 0.96
p = 5.9e-5
HNF4 + CAR+ RXR
n = 1449
r = 0.97
p = 0.04
CTL
TCP
binding per bp per peak
bp from peak center
E
Dual up down HNF4-
n = 88
r = 1.42
p = 7.3e-7
Dual up down HNF4+
n = 169
r = 1.04
p = ns
p = 0.003
Dual down up HNF4-
n = 58
r = 1.18
p = 6.4e-5
Dual down up HNF4+
n = 156
r = 0.97
p = 0.02
p = 0.007
TCP
CTL
binding per bp per peak
bp from peak center
F
Overlapping (<12 bp)
Adjacent (12 – 26 bp)
Separated (>26 bp)
HNF4a
RXR
Relative frequency
Distance to CAR peak center (bp)
G
All
Down up
Up down
Control
TCPOBOP
HNF4
CAR
H4K5Ac
maximum binding per bp per peak
HNF4+
<12
12-26
>26
HNF4-
HNF4 subset
H
Transcript fraction
Net
Up
Down
HNF4:
All
+
-
Reactome 7098628 Metabolism of lipids and lipoproteins
GO:0008610 Lipid biosynthetic process
ko01040 Biosynthesis of unsaturated fatty acids
ko00071 Fatty acid degradation
ko04975 Fat digestion and absorption
Reactome 7099059 Lipoprotein metabolism

Figure 5. HNF4α Binding and Interaction with CAR

(A) HNF4α peak set. The plot shows H4K5Ac$^+$ HNF4α sites with overlays of RXR:CAR and other RXR sites.

(B) Overlap of HNF4α, CAR, and RXR peak sets.

(C) Transcriptional contributions of HNF4α$^+$ and HNF4α$^-$ CAR sites.

(D) Effects of TCPOBOP treatment on HNF4α binding. n, number of peaks in the subset; r, ratio calculated from treated and untreated peak summits; p, p values calculated using paired t tests comparing control and treated values of individual peaks.

(E) Effects of HNF4α on H4K5Ac in *Dual opposite* peak sets. n, r, and p, calculated as above. Boxed p values compare HNF4$^-$ and HNF4$^+$ peak sets, using unpaired t tests of individual peak stimulation ratios.

(F) Average center-center distance of CAR to RXR and HNF4α peaks. The lines indicate positions of overlapping (<12 bp), adjacent (12–26 bp), and separated sites (>26 bp).

(G) Positional effects on HNF4α, CAR, and H4K5Ac levels. HNF4α binding showed minimal change with treatment. HNF4α binding was strongest over the sites that were overlapping or adjacent, although statistical significance was limited by small peak sets. Peak maxima were calculated from histogram analysis. The analyses compared 3 sets: *All* (in subsets), *Dual up down*, and *Dual down up* peaks. HNF4α$^+$ represents all positive peaks, then subdivided into <12-, 12- to 26-, and >26-bp groups. HNF4$^-$ represents all negative peaks. Statistical analysis compared HNF4 levels for individual HNF4$^+$ groups with HNF4 binding of all positive peaks (the 1,009 peak set on the far left) using unpaired t tests; n, the number of peaks in each group; *p < 0.05, **p < 0.01.

(H) Relationship of HNF4α to the ontology of CAR-regulated lipid metabolism. The global lipid gene profile from Figure 3I was elaborated with separate profiles that represent different aspects of lipid metabolism. The plot quantifies TCPOBOP-induced transcriptional changes linked to HNF4$^+$ and HNF4$^-$ CAR peaks. p values for detection of genes within individual profiles: **p <0.01, ***p <0.001, ****p <0.0001, ******p <0.000001.

two purely noncanonical subsets, 58 stimulatory and 112 inhibitory CAR-only peaks that were exclusively linked to 284 genes. Downregulation predominated for these moderately expressed genes while ontology analysis related them to protein modification processes and ion binding, a distinctive phenotypic contribution.

Downregulation via Antagonism of HNF4α

Homodimeric HNF4α shares many gene targets with CAR (Tirona et al., 2003), so we analyzed H4K5Ac-positive HNF4α binding and defined a set of ~10,000 peaks (Figures 5A, S7A, and S7B). The HNF4α peak characterization used restrictions similar to the CAR and RXR peak sets. Of the RXR:CAR peaks 70% coincided with HNF4α peaks (Figures 5A and 5B, Table S4). Regulated genes linked to HNF4α$^-$ RXR:CAR$^+$ peaks showed more total stimulation and less inhibition than those linked to HNF4α$^+$ peaks, even though the latter set contained twice as many genes (Figure 5C). Although these quantifications imply some kind of antagonism, TCPOBOP treatment minimally affected global HNF4α binding, even on RXR:CAR peaks (Figure 5D).

The opposing regulation of *dual opposite* gene pairs suggested a competition that transferred transcriptional initiation and HNF4α had a selective effect on the linked RXR:CAR peaks in these subsets. HNF4α$^-$ peaks showed a strong increase in H4K5Ac, whereas the level was unchanged in HNF4α$^+$ peaks (Figure 5E). This effect was unexpectedly limited to *dual opposite* gene pairs since the increased H4K5Ac of *single up* and *dual up* peaks was independent of HNF4α binding. Similarly, the H4K5Ac levels of *single down* and *dual down* peaks did not change with or without HNF4α (Figure S7C).

One possible explanation for the differential acetylation of HNF4α-positive and HNF4α-negative sites was binding competition with RXR:CAR. To investigate such competition, distances between CAR and HNF4α peak centers were classified to define overlapping (<12 bp center-center distance), adjacent (12–26 bp), or separate (>26 bp) binding sites (Figure 5F). Surprisingly, HNF4α binding was unchanged by TCPOBOP treatment (Figure 5G). The data instead showed the strongest HNF4α binding at overlapping and adjacent sites. The opposing effects of CAR and HNF4α on gene expression thus does not arise from direct binding competition at common sites.

The opposing effects on gene expression of CAR and HNF4α on *dual opposite* gene pairs had strong phenotypic consequences. These are exemplified by ontologic characterization of separate pathways (Figure 5H) within the general profile *cellular lipid metabolic processes* (Figure 3D). CAR binding at HNF4α$^+$ peaks associated with decreased synthesis of some lipids, fatty acids, and lipoproteins. In contrast, CAR binding at HNF4α$^-$ peaks associated with increased fat digestion and absorption, and synthesis of other lipids and lipoproteins.

Common Regulation by a Network of RXR Partners

The antagonism of HNF4α suggested that CAR could have similar effects on other NRs. To evaluate their expression, the entire set of hepatocyte NR was quantified from the RNA-seq libraries along

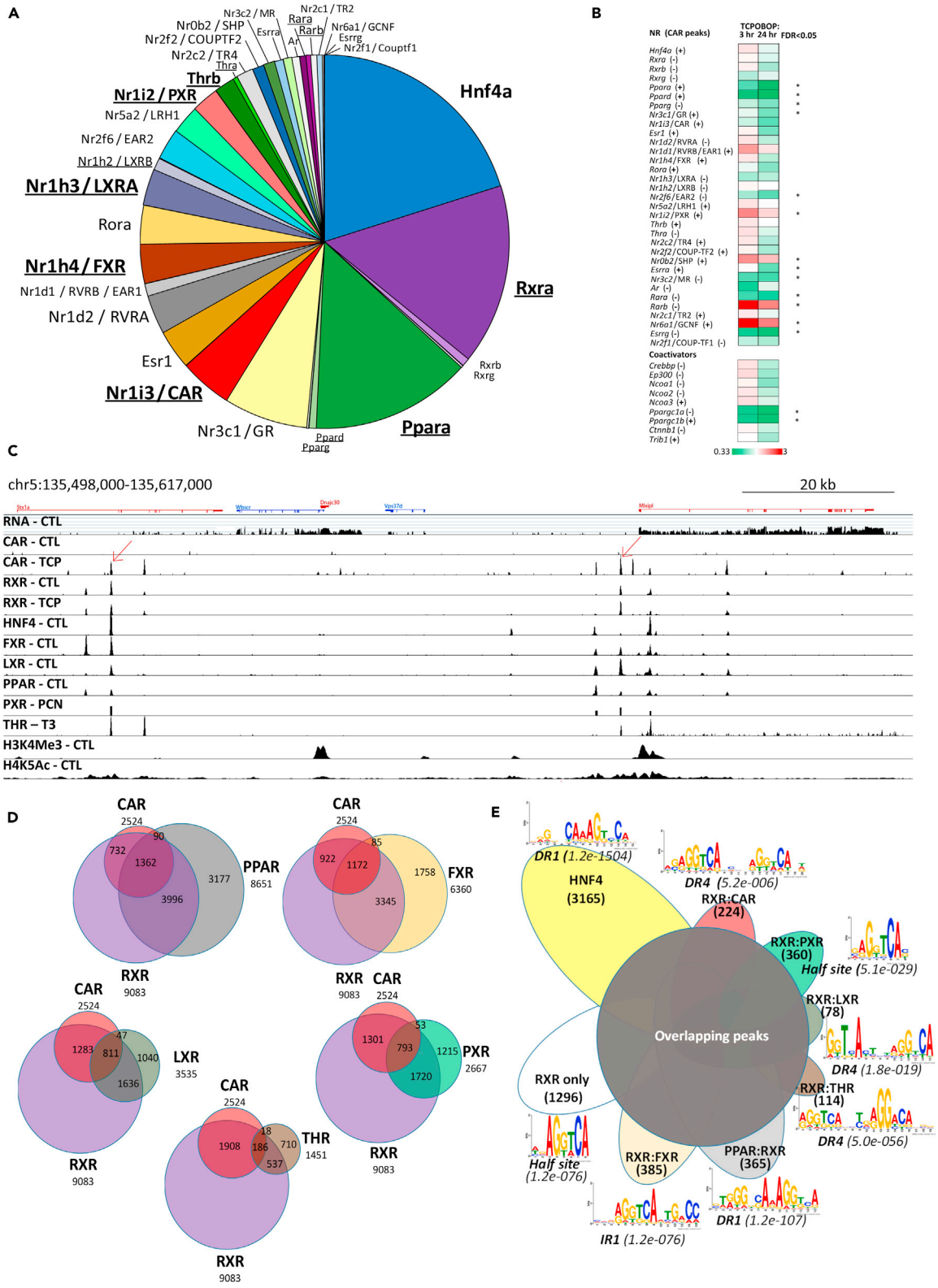
A
Hnf4a
Rxra
Rxrb
Rxrg
Ppara
Pparg
Pparg
Nr3c1 / GR
Nr1i3 / CAR
Esr1
Nr1d2 / RVRA
Nr1d1 / RVRB / EAR1
Nr1h4 / FXR
Rora
Nr1h3 / LXRA
Nr1h2 / LXRB
Nr2f6 / EAR2
Nr5a2 / LRH1
Nr1i2 / PXR
Thrb
Thra
Nr2c2 / TR4
Nr2f2 / COUPTF2
Nr0b2 / SHP
Nr3c2 / MR
Rara
Rarb
Ar
Esrra
Esrrg
Nr6a1 / GCNF
Nr2c1 / TR2
Nr2f1 / Couptf1
B
NR (CAR peaks)
TCPOBOP:
3 hr 24 hr FDR<0.05
Hnf4a (+)
Rxra (-)
Rxrb (-)
Rxrg (-)
Ppara (+)
Ppard (+)
Pparg (-)
Nr3c1/GR (+)
Nr1i3/CAR (+)
Esr1 (+)
Nr1d2/RVRA (-)
Nr1d1/RVRB/EAR1 (+)
Nr1h4/FXR (+)
Rora (+)
Nr1h3/LXRA (-)
Nr1h2/LXRB (-)
Nr2f6/EAR2 (-)
Nr5a2/LRH1 (+)
Nr1i2/PXR (+)
Thrb (+)
Thra (-)
Nr2c2/TR4 (+)
Nr2f2/COUP-TF2 (+)
Nr0b2/SHP (+)
Esrra (+)
Nr3c2/MR (-)
Ar (-)
Rara (-)
Rarb (-)
Nr2c1/TR2 (+)
Nr6a1/GCNF (+)
Esrrg (-)
Nr2f1/COUP-TF1 (-)
Coactivators
Crebbp (-)
Ep300 (-)
Ncoa1 (-)
Ncoa2 (-)
Ncoa3 (+)
Ppargc1a (-)
Ppargc1b (+)
Ctnnb1 (-)
Trib1 (+)
0.33
3
C
chr5:135,498,000-135,617,000
20 kb
RNA - CTL
CAR - CTL
CAR - TCP
RXR - CTL
RXR - TCP
HNF4 - CTL
FXR - CTL
LXR - CTL
PPAR - CTL
PXR - PCN
THR – T3
H3K4Me3 - CTL
H4K5Ac - CTL
D
CAR
2524
90
732
1362
3996
3177
PPAR
8651
RXR
9083
CAR
2524
85
922
1172
3345
1758
FXR
6360
RXR
9083
CAR
2524
47
1283
811
1040
1636
LXR
3535
RXR
9083
CAR
2524
53
1301
793
1215
1720
PXR
2667
RXR
9083
CAR
2524
18
1908
186
710
537
THR
1451
RXR
9083
E
DR1 (1.2e-1504)
HNF4
(3165)
DR4 (5.2e-006)
RXR:CAR
(224)
RXR:PXR
(360)
Half site (5.1e-029)
RXR:LXR
(78)
DR4 (1.8e-019)
Overlapping peaks
RXR only
(1296)
RXR:THR
(114)
DR4 (5.0e-056)
Half site
(1.2e-076)
RXR:FXR
(385)
PPAR:RXR
(365)
DR1 (1.2e-107)
IR1 (1.2e-076)

Figure 6. CAR Regulatory and Binding Relationships with Other RXR Partners

(A) Relative abundance of NR transcripts in normal hepatocytes. Levels were determined from RNA-seq analysis (Table S3). RXR partners are underlined.

(B) Regulation following TCPOBOP treatment. The heatmaps show 3-hr and 24-hr average changes. +, linked CAR binding within 400 kb; –, no linked CAR binding; *, false discovery rate (< 0.05 for the expression time series.

(C) CAR and other NRs bind near ChREBP/Mlxipl. Note strongly induced CAR binding on $HNF4^{+}$ and $HNF4^{-}$ sites that overlap with RXR, FXR, LXR, PXR, and THR (arrows, 66 and 2.4 kb from the Mlxipl TSS). The tracks show RNA-seq, ChIP-seq alignments, and previously compiled PXR peaks.

(D) Overlap of CAR, RXR, and other NR peaks. PPAR, LXR, and FXR represent basal expression, PXR after pregnenolone 16α-carbonitrile treatment, and THR after T3-treatment. Filtering removed peaks with $p > 0.001$, the bottom 3% of the range of binding strength, or absence of H4K5Ac.

(E) MEME-ChIP analysis. Overlapping peaks generated only half-site motifs, but subsets that uniquely bound CAR, HNF4α, PPAR, FXR, or LXR generated characteristic paired motifs, which validated the identification and filtering processes for each factor. Non-overlapping RXR peaks gave only a half-site motif, suggesting heterogeneity due to unidentified binding partners. Non-overlapping PXR peaks only generated a half-site motif closely related to CAR. For each NR motif, the class of binding site is shown in bold type and the E value in parentheses.

with selected coregulators (Figures 6A and 6B). Strong effects on *Ppara* and the coregulator *Ppargc1b* were notable, each with downregulation of about 60% that was associated with nearby RXR:CAR binding.

Since PPAR, FXR, and LXR are all activated by endogenous ligands, we compiled peak sets of the basal state from published datasets (Boergesen et al., 2012; Thomas et al., 2010). ChIP-seq data was also obtained from a THR study that compared hypothyroid propylthiouracil-treated mice with and without T3 for 5 days (Grontved et al., 2015) and from a PXR study that characterized livers 12 hr after a single dose of pregnenolone 16α-carbonitrile (Cui et al., 2010). For the latter, we used a compiled peak set (Julia Cui, personal communication). All sets received the same filtering and cutoffs as our own datasets. For basal PPAR, FXR, and LXR, H4K5Ac filtering removed 13%, 9%, and 7%, compared with the 14% removed from the CAR peak set. H4K5Ac filtering of PXR and THR peak sets removed greater proportions of peaks, 17% and 44%, respectively.

Throughout the genome, the NR peaks frequently overlapped. For example, the 80-kb region upstream of ChREBP/Mlxipl—an important transcription factor that integrates glycolysis and lipogenesis—displayed CAR, HNF4, RXR, FXR, LXR, PPAR, PXR, and THR peaks, overlapping in different combinations (Figure 6C).

Overlap of these RXR partners with CAR was frequent (Figure 6D, Table S4). PPARα formed the largest set of RXR dimeric peaks (5,358) and also had the largest overlap fraction with RXR:CAR peaks, 65%. Other overlap fractions were FXR, 56%; LXR, 39%; PXR, 39%; and THR, 9%. MEME analysis of overlapping subsets yielded only NR half-site motifs (not illustrated). In contrast, MEME generated characteristic dimeric motifs for non-overlapping CAR, PPAR, FXR, LXR, THR, and HNF4α sites that validated the peak compilations (Figure 6E). PXR and RXR peaks were exceptions. Their non-overlapping sets were probably heterogeneous since they generated only half-site motifs. Compared to the 17% of CAR-only peaks, the PPAR, FXR, LXR, PXR, and THR analyses demonstrated more RXR^{-} peaks, 28%–50%. These RXR^{-} peaks—NR-specific noncanonical binding or technical differences among diverse datasets—were filtered before comparative analysis. The distribution of binding peaks, representation of known binding sites, and linkage to regulated genes all indicated that the peak sets were adequate for correlation of their binding in liver.

Phenotypic Effects of Coregulation by CAR and Other NR

Since acetylation of the *dual opposite* peaks provided a sensitive assessment of antagonism by HNF4, we used these peak sets to analyze interactions with PPAR, FXR, LXR, PXR, and THR (Figure 7A). Peaks with CAR and a second NR always had higher basal acetylation, presumably reflecting their activation by both. However, sites that lacked PPAR or FXR—like those that lacked HNF4α—showed lower basal acetylation and stronger stimulation of acetylation by TCPOBOP. These acetylation states discriminated antagonism of CAR and the other NR but did not explain the antagonism because high acetylation was maintained. For LXR and THR, treatment gave nearly equivalent stimulation of positive and negative sites, a neutral relationship. PXR distinctively showed a cooperative relationship with CAR, since TCPOBOP stimulated acetylation of PXR-positive more than PXR-negative peaks.

Further analysis resolved the effects of a second cobinding NR from those of HNF4α, which bound to many of the same peaks (Figure 7B). The inhibition of acetylation by PPARα and FXR was even greater than the inhibition by HNF4α, consistent with strong antagonism of CAR. Again, LXR and THR were neutral, and PXR

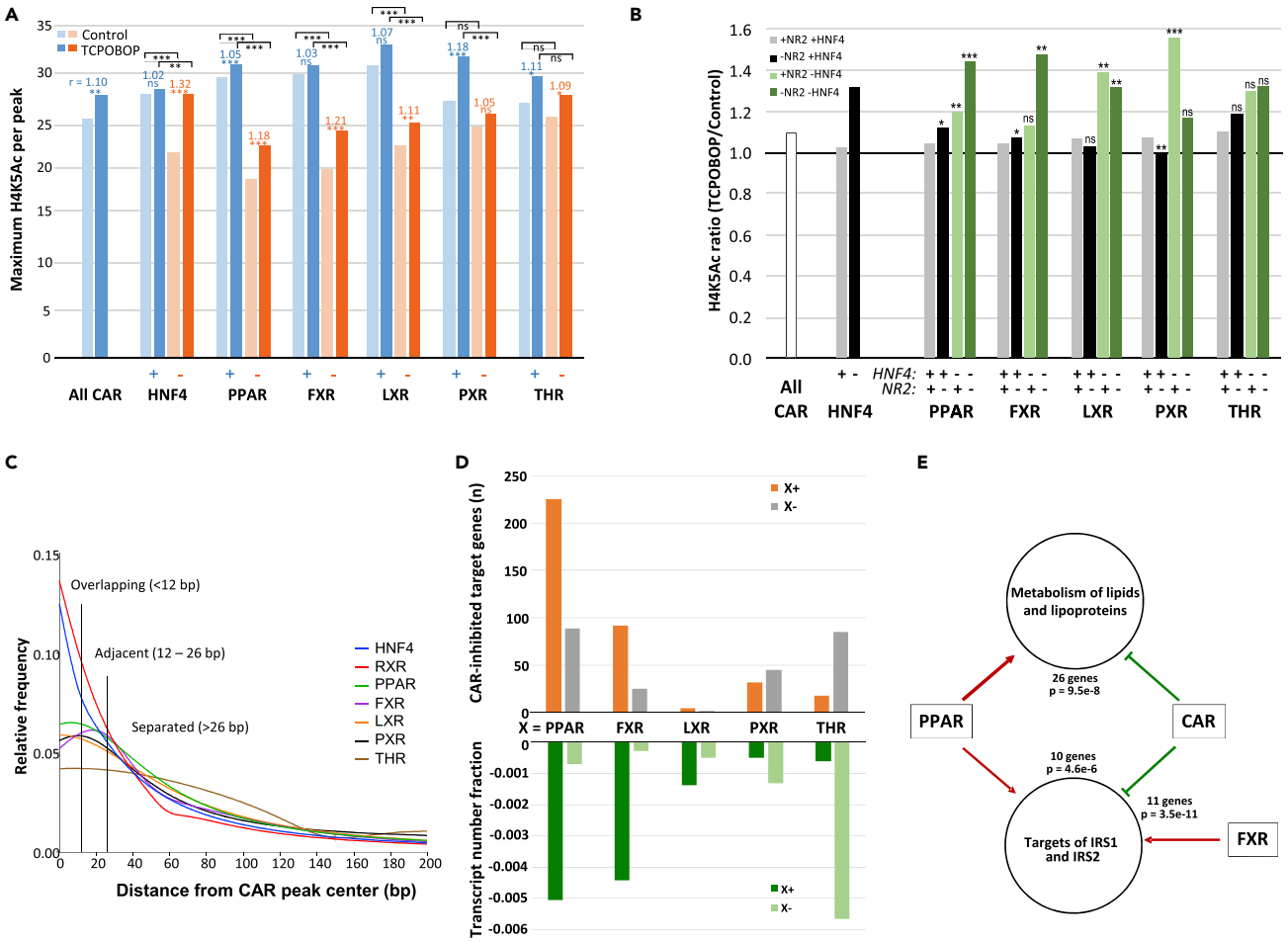

Figure 7. Effects of Second NR at CAR-Binding Peaks

(A) Effects of a second NR on *Dual opposite* CAR peaks. Levels of H4K5Ac were plotted as histogram peak summits, whereas statistical analysis compared the values of individual peaks. The summit ratios (treated/control) are listed in color with p values from paired t tests. Brackets mark separate comparisons of basal and TCPOBOP-stimulated expression, from unpaired t tests. **p < 0.01, ***p < 0.001; ns, not significant.

(B) Resolution of the effects of a second NR from HNF4α. The plots show the ratios of TCPOBOP-treated to control histogram summits. For each second NR (NR2), ratios sets were compared with peaks that had both receptors (HNF4$^+$, NR2$^+$) using unpaired t tests. *p < 0.05, **p < 0.01, ***p < 0.001.

(C) Distribution of second NR sites in CAR-binding enhancers. The vertical lines indicate positions of overlapping (<12 bp), adjacent sites (12–26 bp), and separated sites (>26 bp).

(D) CAR-linked genes with inhibition by TCPOBOP but stimulation by a ligand for the second NR. Histograms show the number of genes and magnitude of inhibition, displayed as transcript number fraction. X+, genes regulated by peaks that bind both CAR and the second NR; X-, genes regulated by separate peaks that bind CAR and the second NR.

(E) CAR-PPARα and CAR-FXR antagonism in the regulation of lipid metabolism and insulin signaling. Overviews of these ontology profiles are presented in Figure 3D.

showed cooperation with CAR. Comparison of peak centers showed that some cobinding NR directly overlapped with CAR (Figure 7C). However, NR position within enhancers showed little relationship to stimulation of H4K5Ac (not illustrated).

An assessment of phenotypic effects then correlated CAR-linked genes with published expression profiles of PPAR, FXR, LXR, PXR, and THR (Boergesen et al., 2012; Grontved et al., 2015; Oshida et al., 2015; Rakhshandehroo et al., 2007; Zhan et al., 2014). Individual CAR-linked genes in these profiles showed either concordant or discordant regulation by the second NR (Table S5, Figure 7D). In the two largest discordant sets, CAR shared 225 and 92 enhancers with PPARα and FXR, respectively. In contrast, CAR inhibition of genes stimulated by PXR or THR linked to separate enhancers. Phenotypically, the antagonistic binding of CAR suggested important metabolic consequences, inhibition of lipid metabolism genes stimulated

by PPARα and IRS response genes stimulated by both PPARα and FXR (Figure 7E; Cipriani et al., 2010; Guo et al., 2009; Kim and Moore, 2017).

DISCUSSION

Modeling CAR Regulation

The studies in this article correlated genome-wide CAR binding in the liver with changes in the hepatocyte transcriptome. In the absence of specific perturbation of individual sites and genes, such analysis can only be correlative. The analysis used unbiased strategies to enrich the quality of these correlations. The article also provides resources with full data on each CAR peak and regulated gene (Tables S3 and S4).

Peak sets were refined by eliminating those that represented library artifacts, low statistical significance, weak binding, and lack of association with activate chromatin. The most important refinement was the elimination of weak binding sites despite the statistical significance of most of these detections. Elimination was justified by their weak interaction and poor correlation with binding-site motif analysis and gene regulation. Statistical restriction, even to very low p values, did not eliminate most weak sites (see Figures S3A–S3C and S7A). The final sets of 2,500 CAR peaks (2,100 RXR:CAR peaks), 9,100 RXR peaks, and 10,000 HNF4α peaks are highly representative of observed hepatocyte gene regulation.

Transcriptome correlation used comparable refinement, first by limiting analysis to hepatocyte-expressed CAR-linked genes regulated by TCPOBOP treatment. More specialized restrictions were necessary to enrich specific regulatory relationships: two genes closest to each induced CAR-binding peak (~2,500 genes) and CAR peak subsets with defined linkage to either up or down 24-hr average regulation (~1,600 peaks). Despite the relatively small size of these sets, they still related 80% of RXR:CAR peaks to 70% of the CAR-linked change in transcriptional initiation. The aggregate measurement of H4K5Ac in these sets showed different effects if peaks were linked to gene pairs with up, down, or opposite regulation. The separate H4K5Ac relationships validate the unbiased selection criteria and indicate a high degree of homogeneous enrichment.

The analyses led to a specific view of gene regulation in mature liver. CAR did not activate a program of differentiation or repression. Changes in gene expression, even the strongest, linked to sites that already bound RXR within hypersensitive regions surrounded by acetylated chromatin. CAR therefore modulated active genes within the mature liver phenotype. Modulation of active genes also characterized liver regulation by other RXR partners.

Properties of CAR Regulation

The minimal CAR binding in control liver presumably reflected a low level of endogenous or dietary ligands. Nevertheless, the vast majority of heterodimeric sites (92%) were occupied by RXR before TCPOBOP treatment, suggesting prior regulation by other NR:RXR pairs. In addition, many of the ~7,000 "CAR-negative" RXR peaks actually showed weak CAR binding that reflects the moderate differences in specificity of NR-binding sites.

Most CAR peaks corresponded to distant enhancers, typical of gene regulation by NR. Use of a 400-kb distance cutoff led to inclusion of a few interesting regulations, but few regulatory peaks were very distant and quantifications using a 150-kb distance cutoff were virtually the same (not shown).

The aggregate analysis of large peak sets in some ways contradicts the examination of exceptional candidate genes, which may have outlying properties. To examine their special regulatory mechanisms, we investigated a variety of outlying subsets for correlation with other NR binding, chromatin acetylation, binding motifs, gene expression, and ontology. The outlier CAR peak sets had basal liver detection (245 peaks), unusually strong binding (263 peaks), *de novo* binding of RXR and CAR (99 peaks), or a >2-fold change in acetylation, up (48 peaks) or down (19 peaks). The strongly binding peaks had a moderate positive correlation with the strength of gene induction after TCPOBOP treatment and generated the clearest binding motif, but none of the other outlying subsets showed a significant correlation with differences in a second property or with ontology profiles. Moreover, genes regulated by these outliers often associated with additional peaks that were more typical.

Transcriptional Antagonism of CAR with Other NR

Most CAR peaks overlapped with HNF4α or other NR. Regardless of this overlap, peaks associated with upregulated genes increased acetylation. CAR activation also induced downregulation, but the mechanism was not clear. CAR peaks associated with oppositely regulated genes provided a valuable resource for examining this mechanism since opposing regulation suggested transfer rather than loss of activation. In these *dual opposite* CAR peaks, increased acetylation inversely correlated with HNF4α (or other NR) binding. Thus, downregulation could be mediated by competition between HNF4α and CAR. Binding site occupancy, however, was not decreased even when sites directly overlapped. Instead, overlapping binding sites had the strongest binding of both CAR and HNF4α. The likely explanation for the lack of binding competition is *site sharing*, which can occur if the time of residency is brief. Moreover, binding of one NR at a shared site can increase occupancy by a second via *assisted loading* if the first has modified chromatin to improve accessibility (Voss et al., 2011). Short residency time and assisted loading, however, still do not explain transcriptional downregulation or the apparent competition for expression of nearby genes.

It is important to consider two alternate explanations for overlapping binding. The first is that different NRs might bind in separate cell populations. This explanation is incompatible with the observed interactions of CAR with HNF4α, PPAR, and FXR (Figures 5E, 7A, and 7B). Functional relationships with LXR, PXR, and THR are more ambiguous, but coexpression of these NRs with CAR in the same hepatocytes is well known. The second explanation is that binding of CAR might be indirect. Indeed, indirect CAR binding to CEBP is likely for CAR-only sites, but indirect binding of CAR to bound HNF4α dimers is unlikely. Moreover, the occupied sites bind CAR, HNF4α, and RXR and have canonical dimeric binding motifs compatible for either RXR:CAR or HNF4α.

The NRs of this study (Figure 8A) share domain structure, dimeric binding to similar paired half-sites, and activation through the LBD and its AF2 region. In the typical activation process, the LBD recruits a p160 coactivator that acetylates histones at several sites including H4K5 (Li et al., 2003). The LBD and p160 then recruit CBP and other coregulators to further modify chromatin, link to a distant promoter, and stimulate the formation of a preinitiation complex (Rosenfeld et al., 2006). CAR and HNF4α constitutively mediate this LBD-driven process; PPAR, FXR, LXR, PXR, and THR require an activating ligand; and RXR is usually considered a passive partner (Evans and Mangelsdorf, 2014). Except for PXR (and CAR), however, activating ligands are normally present in the liver.

NRs share a common activation mechanism through the LBD and its coactivators. A second NR on the same enhancer might compete for these coactivators but would then have an equivalent transcriptional effect. Coactivator competition could, however, explain how CAR downregulates unlinked genes, an effect suggested by the reduced acetylation of CAR-negative RXR sites (Figure 2G).

Many NRs have a second activation domain (AF1) at the N terminal. AF1 domains differ and can provide specific mechanisms for individual NR. CAR is the most compact NR in this study, without an N-terminal domain or AF1. The functions of some AF1 regions are uncharacterized, but two other hepatocyte NRs have known special features. TRIB1 and CTNNB1 are AF1-specific cofactors for HNF4α and FXR, respectively (Liu et al., 2015; Soubeyrand et al., 2017). HNF4α also has a distinctive F-domain at the C terminal that modulates the function of AF2 (Sladek et al., 1999).

NR competition, for binding or coactivators, does not explain downregulation or the reciprocal changes of genes linked to the same enhancers. *Gene competition*, the competition of promoters for local enhancers, provides an alternative mechanism that can explain the behavior of opposite gene pairs (Bulger and Groudine, 1999; Quintero-Cadena and Sternberg, 2016). Several observations are consistent. (1) The great majority of regulated promoters are distant from their CAR-binding enhancers. Moreover, 378 regulated gene pairs—including 225 with opposite regulation—link to single CAR-binding peaks. (2) The opposite regulation of gene pairs suggests that activation shifts from one gene to the other. (3) Downregulating enhancers are farther from the promoters than upregulating enhancers (Figures 3C and S4E), suggesting that promoter distance affects competition.

We therefore hypothesize that an additional NR will alter the competition for local promoters to increase diversion of an enhancer to a second gene. This will downregulate the first and upregulate the second (Figure 8B). The effect on local gene competition can be small or substantial for individual genes and maintains

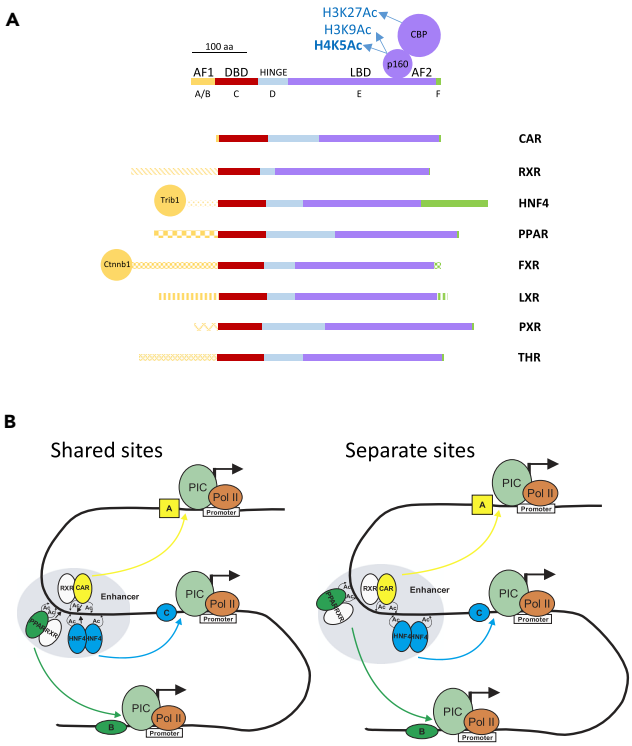

Figure 8. Gene Competition via Selective Properties of NR Dimers

(A) Common and distinctive features of individual NR. Top, general domains and binding partners; bottom, individual NR and specialized AF1 partners. The domains that mediate DNA binding (DBD), dimerization, and ligand binding (LBD) are very similar among NRs. The LBD and its AF2 region mediates transcriptional activation, starting with direct binding of p160 coactivators that bind CBP and other partners. p160s and CBP are acetylases that modify H4K5, H3K9, H3K27, and other targets. Divergent N-terminal AF1 domains mediate transcriptional activation by mechanisms specific for individual NR.

(B) A model for modulating expression via gene competition in which alternative NRs have different affinities for local promoters. Instead of competing, NRs share overlapping binding sites, which have stronger binding than separated sites. Without competition, each NR would have only a positive effect on histone acetylation around the enhancer. Binding at overlapping or separate sites would have comparable effects on enhancer function.

a regional balance of expression. The effects result from a shift of activation and modulate an established phenotype without changing it.

As an example, changes in the lipoprotein *Apoa1*, *Apoc3*, *Apoa4* and *Apoa5* gene cluster made large contributions to the transcription fraction. The 4 genes cluster in a 43-kb region of chromosome 9 with 2 CAR peaks—one HNF4α^+ and both PPAR$^+$, FXR$^+$, and PXR$^+$. In response to TCPOBOP, expression of *Apoa1* (1.3 X) and *Apoa4* (4.1 X) went up, whereas that of *Apoc3* (0.8 X) and *Apoa5* (0.8 X) went down.

Relationship to Other NRs

The most prominent CAR-NR interaction was with HNF4α, an essential regulator of early liver development and the mature hepatocyte phenotype (Parviz et al., 2003). HNF4α and CAR share many target genes through ~1,400 common enhancers. However, constitutive HNF4α activation does not change in response to physiologic signals or ligands (Yuan et al., 2009). CAR and the other RXR partners therefore mediate dynamic change by competing within, and borrowing transcriptional resources from, the HNF4α-controlled phenotype.

NR-controlled gene competition can account for the reciprocal stimulation and inhibition between the fed and fasted states mediated by FXR and PPARα (Kim and Moore, 2017). These NRs have common binding sites near "more than 1,100 target genes that showed opposite responses much more frequently than concordant responses." CAR also modulates these responses, since ~1,000 peaks bind PPAR, FXR, and

CAR. CAR-mediated downregulation of *targets of IRS1 and IRS2*, a profile derived from $Irs1^{-/-}$ and $Irs2^{-/-}$ mice, highlights its antagonism of FXR and PPARα (Cipriani et al., 2010; Guo et al., 2009; Guerre-Millo et al., 2001). CAR also antagonizes PPAR by a second significant effect, transcriptional downregulation of *Ppara*.

Drug Responses Are Different from Ordinary Metabolic Regulation

A critical property that discriminates CAR from HNF4α and other RXR partners is its inactivity in basal liver. The induced CAR response is very strong and thus diverts the normal regulatory network. The combination of metabolic reprioritization with rapid hepatocyte growth and proliferation suggests that the CAR response evolved to deactivate toxic agents and quickly replace the hepatocytes that they kill.

The RXR network normally regulates metabolic genes that respond to cyclic stimuli from feeding and activity. The network coordinates the timing of these responses and balances the utilization of limiting transcriptional resources (Kim and Moore, 2017). Drugs are a special class of xenobiotics, selected because they are relatively nontoxic and have valuable therapeutic properties. CAR-induced proteins like p450 cytochromes inactivate these drugs, but CAR also rebalances the metabolism of lipids and glucose tolerance. Maintaining a significant drug level can therefore apply a continuous perturbation to the cyclic regulatory networks and produce metabolic changes, off-target side effects that are unrelated to the direct action of the inducing drug.

Limitations of the Study

This study focused on short-term changes to show how CAR controls liver metabolism. The study was deliberately limited to female mice to simplify the analysis of this sexually dimorphic response. Species differences are also important, since differences among the responses of mouse, rat, and human livers are well known. Moreover, CAR activation in a natural setting may associate with toxic agents that cause liver damage, which will significantly modify the response. These important biological differences must be characterized in future studies, particularly to understand human responses and their application to therapy.

At a mechanistic level, our analysis could only correlate CAR binding at distant enhancers with changes in gene expression because there was no demonstration that modification of specific enhancers altered the activation of putative target genes and there was no analysis of enhancer-promoter contact. The data also suggest that enhancers can interact with each other, a similar kind of linked interaction. Indeed, the relationships among promoters and distant enhancers are frequently ambiguous. Although beyond the scope of this article, more specific characterization of these interactions is an important area for new research.

Another limitation was our use of specific chromatin acetylations to characterize changes induced by CAR binding. The main analysis of H4K5Ac had a strong mechanistic link to NR activation, gave clear quantifiable changes, and provided distinctive correlations with types of gene expression. Nevertheless, the integrated study of H4K5Ac, H3K27Ac, H3K9Ac, DHS, and other chromatin modifications, could provide a detailed view of the progressive enhancer changes that lead to transcriptional activation following NR binding. CAR has rapid and strong induction from a minimal basal state in the liver and therefore provides an ideal system for such studies of natural transcriptional activation *in vivo*.

METHODS

All methods can be found in the accompanying Transparent Methods supplemental file.

SUPPLEMENTAL INFORMATION

Supplemental Information includes Transparent Methods, seven figures, and five tables and can be found with this article online at https://doi.org/10.1016/j.isci.2018.10.018.

ACKNOWLEDGMENTS

The studies were supported by NIH grant CA104292. We are grateful to Shahina Maqbool and the Epigenetics Shared Facility of Albert Einstein College of Medicine for outstanding sequencing and frequent guidance; Eric Bouhassira, Albert Einstein College of Medicine, for introducing us to ChIP-seq and its visualization; Julia Cui, University of Washington, for the compiled PXR peak sets; and Andrew Althouse, University of Pittsburgh, for statistical advice and computation.

AUTHOR CONTRIBUTIONS

Conceptualization, J.T. and J.L.; Methodology, J.T., R.M., and C.J.; Investigation, J.T., R.M., C.J., and J.L.; Writing – Original Draft, J.L.; Writing – Review & Editing, J.T and J.L.; Funding Acquisition, J.L.; Resources, J.T., R.M., and C.J.; Supervision, J.L.

DECLARATION OF INTERESTS

The authors declare no competing interests.

Received: March 12, 2018
Revised: August 2, 2018
Accepted: October 16, 2018
Published: November 30, 2018

REFERENCES

Bailey, T.L., Johnson, J., Grant, C.E., and Noble, W.S. (2015). The MEME suite. Nucleic Acids Res. *43*, W39–W49.

Boergesen, M., Pedersen, T.A., Gross, B., van Heeringen, S.J., Hagenbeek, D., Bindesboll, C., Caron, S., Lalloyer, F., Steffensen, K.R., Nebb, H.I., et al. (2012). Genome-wide profiling of liver X receptor, retinoid X receptor, and peroxisome proliferator-activated receptor alpha in mouse liver reveals extensive sharing of binding sites. Mol. Cell. Biol. *32*, 852–867.

Bulger, M., and Groudine, M. (1999). Looping versus linking: toward a model for long-distance gene activation. Genes Dev. *13*, 2465–2477.

Choi, H.S., Chung, M., Tzameli, I., Simha, D., Lee, Y.K., Seol, W., and Moore, D.D. (1997). Differential transactivation by two isoforms of the orphan nuclear hormone receptor CAR. J. Biol. Chem. *272*, 23565–23571.

Cipriani, S., Mencarelli, A., Palladino, G., and Fiorucci, S. (2010). FXR activation reverses insulin resistance and lipid abnormalities and protects against liver steatosis in Zucker (fa/fa) obese rats. J. Lipid Res. *51*, 771–784.

Columbano, A., Ledda-Columbano, G.M., Pibiri, M., Cossu, C., Menegazzi, M., Moore, D.D., Huang, W., Tian, J., and Locker, J. (2005). Gadd45beta is induced through a CAR-dependent, TNF-independent pathway in murine liver hyperplasia. Hepatology *42*, 1118–1126.

Cui, J.Y., Gunewardena, S.S., Rockwell, C.E., and Klaassen, C.D. (2010). ChIPing the cistrome of PXR in mouse liver. Nucleic Acids Res. *38*, 7943–7963.

Cui, J.Y., and Klaassen, C.D. (2016). RNA-Seq reveals common and unique PXR- and CAR-target gene signatures in the mouse liver transcriptome. Biochim. Biophys. Acta *1859*, 1198–1217.

Evans, R.M., and Mangelsdorf, D.J. (2014). Nuclear receptors, RXR, and the big bang. Cell *157*, 255–266.

Fang, B., Mane-Padros, D., Bolotin, E., Jiang, T., and Sladek, F.M. (2012). Identification of a binding motif specific to HNF4 by comparative analysis of multiple nuclear receptors. Nucleic Acids Res. *40*, 5343–5356.

Feng, J., Liu, T., Qin, B., Zhang, Y., and Liu, X.S. (2012). Identifying ChIP-seq enrichment using MACS. Nat. Protoc. *7*, 1728–1740.

Grontved, L., Waterfall, J.J., Kim, D.W., Baek, S., Sung, M.H., Zhao, L., Park, J.W., Nielsen, R., Walker, R.L., Zhu, Y.J., et al. (2015). Transcriptional activation by the thyroid hormone receptor through ligand-dependent receptor recruitment and chromatin remodelling. Nat. Commun. *6*, 7048.

Guerre-Millo, M., Rouault, C., Poulain, P., Andre, J., Poitout, V., Peters, J.M., Gonzalez, F.J., Fruchart, J.C., Reach, G., and Staels, B. (2001). PPAR-alpha-null mice are protected from high-fat diet-induced insulin resistance. Diabetes *50*, 2809–2814.

Guo, S., Copps, K.D., Dong, X., Park, S., Cheng, Z., Pocai, A., Rossetti, L., Sajan, M., Farese, R.V., and White, M.F. (2009). The Irs1 branch of the insulin signaling cascade plays a dominant role in hepatic nutrient homeostasis. Mol. Cell. Biol. *29*, 5070–5083.

Heinz, S., Benner, C., Spann, N., Bertolino, E., Lin, Y.C., Laslo, P., Cheng, J.X., Murre, C., Singh, H., and Glass, C.K. (2010). Simple combinations of lineage-determining transcription factors prime cis-regulatory elements required for macrophage and B cell identities. Mol. Cell *38*, 576–589.

Kawamoto, T., Sueyoshi, T., Zelko, I., Moore, R., Washburn, K., and Negishi, M. (1999). Phenobarbital-responsive nuclear translocation of the receptor CAR in induction of the CYP2B gene. Mol. Cell. Biol. *19*, 6318–6322.

Kim, K.H., and Moore, D.D. (2017). Regulation of liver energy balance by the nuclear receptors farnesoid X receptor and peroxisome proliferator activated receptor alpha. Dig. Dis. *35*, 203–209.

Kobayashi, K., Hashimoto, M., Honkakoski, P., and Negishi, M. (2015). Regulation of gene expression by CAR: an update. Arch. Toxicol. *89*, 1045–1055.

Lajugie, J., and Bouhassira, E.E. (2011). GenPlay, a multipurpose genome analyzer and browser. Bioinformatics *27*, 1889–1893.

Ledda-Columbano, G.M., Pibiri, M., Concas, D., Molotzu, F., Simbula, G., Cossu, C., and Columbano, A. (2003). Sex difference in the proliferative response of mouse hepatocytes to treatment with the CAR ligand, TCPOBOP. Carcinogenesis *24*, 1059–1065.

Li, X., Wong, J., Tsai, S.Y., Tsai, M.J., and O'Malley, B.W. (2003). Progesterone and glucocorticoid receptors recruit distinct coactivator complexes and promote distinct patterns of local chromatin modification. Mol. Cell. Biol. *23*, 3763–3773.

Liu, X., Zhang, X., Ji, L., Gu, J., Zhou, M., and Chen, S. (2015). Farnesoid X receptor associates with beta-catenin and inhibits its activity in hepatocellular carcinoma. Oncotarget *6*, 4226–4238.

Locker, J., Tian, J., Carver, R., Concas, D., Cossu, C., Ledda-Columbano, G.M., and Columbano, A. (2003). A common set of immediate-early response genes in liver regeneration and hyperplasia. Hepatology *38*, 314–325.

Oshida, K., Vasani, N., Thomas, R.S., Applegate, D., Gonzalez, F.J., Aleksunes, L.M., Klaassen, C.D., and Corton, J.C. (2015). Screening a mouse liver gene expression compendium identifies modulators of the aryl hydrocarbon receptor (AhR). Toxicology *336*, 99–112.

Parviz, F., Matullo, C., Garrison, W.D., Savatski, L., Adamson, J.W., Ning, G., Kaestner, K.H., Rossi, J.M., Zaret, K.S., and Duncan, S.A. (2003). Hepatocyte nuclear factor 4alpha controls the development of a hepatic epithelium and liver morphogenesis. Nat. Genet. *34*, 292–296.

Pasini, D., Malatesta, M., Jung, H.R., Walfridsson, J., Willer, A., Olsson, L., Skotte, J., Wutz, A., Porse, B., Jensen, O.N., et al. (2010). Characterization of an antagonistic switch between histone H3 lysine 27 methylation and acetylation in the transcriptional regulation of Polycomb group target genes. Nucleic Acids Res. *38*, 4958–4969.

Quintero-Cadena, P., and Sternberg, P.W. (2016). Enhancer sharing promotes neighborhoods of transcriptional regulation across eukaryotes. G3 (Bethesda) *6*, 4167–4174.

Rakhshandehroo, M., Sanderson, L.M., Matilainen, M., Stienstra, R., Carlberg, C., de Groot, P.J., Muller, M., and Kersten, S. (2007). Comprehensive analysis of PPARalpha-dependent regulation of hepatic lipid

metabolism by expression profiling. PPAR Res. *2007*, 26839.

Rosenfeld, M.G., Lunyak, V.V., and Glass, C.K. (2006). Sensors and signals: a coactivator/corepressor/epigenetic code for integrating signal-dependent programs of transcriptional response. Genes Dev. *20*, 1405–1428.

Sladek, F.M., Ruse, M.D., Jr., Nepomuceno, L., Huang, S.M., and Stallcup, M.R. (1999). Modulation of transcriptional activation and coactivator interaction by a splicing variation in the F domain of nuclear receptor hepatocyte nuclear factor 4alpha1. Mol. Cell. Biol. *19*, 6509–6522.

Soubeyrand, S., Martinuk, A., and McPherson, R. (2017). TRIB1 is a positive regulator of hepatocyte nuclear factor 4-alpha. Sci. Rep. *7*, 5574.

Spencer, T.E., Jenster, G., Burcin, M.M., Allis, C.D., Zhou, J., Mizzen, C.A., McKenna, N.J., Onate, S.A., Tsai, S.Y., Tsai, M.J., et al. (1997). Steroid receptor coactivator-1 is a histone acetyltransferase. Nature *389*, 194–198.

Suino, K., Peng, L., Reynolds, R., Li, Y., Cha, J.Y., Repa, J.J., Kliewer, S.A., and Xu, H.E. (2004). The nuclear xenobiotic receptor CAR: structural determinants of constitutive activation and heterodimerization. Mol. Cell *16*, 893–905.

Thomas, A.M., Hart, S.N., Kong, B., Fang, J., Zhong, X.B., and Guo, G.L. (2010). Genome-wide tissue-specific farnesoid X receptor binding in mouse liver and intestine. Hepatology *51*, 1410–1419.

Tian, J., Huang, H., Hoffman, B., Liebermann, D.A., Ledda-Columbano, G.M., Columbano, A., and Locker, J. (2011). Gadd45β is an inducible coactivator of transcription that facilitates rapid liver growth in mice. J. Clin. Invest. *121*, 4491–4502.

Tie, F., Banerjee, R., Stratton, C.A., Prasad-Sinha, J., Stepanik, V., Zlobin, A., Diaz, M.O., Scacheri, P.C., and Harte, P.J. (2009). CBP-mediated acetylation of histone H3 lysine 27 antagonizes Drosophila Polycomb silencing. Development *136*, 3131–3141.

Tirona, R.G., Lee, W., Leake, B.F., Lan, L.B., Cline, C.B., Lamba, V., Parviz, F., Duncan, S.A., Inoue, Y., Gonzalez, F.J., et al. (2003). The orphan nuclear receptor HNF4alpha determines PXR- and CAR-mediated xenobiotic induction of CYP3A4. Nat. Med. *9*, 220–224.

Tzameli, I., Pissios, P., Schuetz, E.G., and Moore, D.D. (2000). The xenobiotic compound 1,4-bis[2-(3,5-dichloropyridyloxy)]benzene is an agonist ligand for the nuclear receptor CAR. Mol. Cell. Biol. *20*, 2951–2958.

Uslu, V.V., Petretich, M., Ruf, S., Langenfeld, K., Fonseca, N.A., Marioni, J.C., and Spitz, F. (2014). Long-range enhancers regulating Myc expression are required for normal facial morphogenesis. Nat. Genet. *46*, 753–758.

Voss, T.C., Schiltz, R.L., Sung, M.H., Yen, P.M., Stamatoyannopoulos, J.A., Biddie, S.C., Johnson, T.A., Miranda, T.B., John, S., and Hager, G.L. (2011). Dynamic exchange at regulatory elements during chromatin remodeling underlies assisted loading mechanism. Cell *146*, 544–554.

Waxman, D.J., Dannan, G.A., and Guengerich, F.P. (1985). Regulation of rat hepatic cytochrome P-450: age-dependent expression, hormonal imprinting, and xenobiotic inducibility of sex-specific isoenzymes. Biochemistry *24*, 4409–4417.

Wei, P., Zhang, J., Egan-Hafley, M., Liang, S., and Moore, D.D. (2000). The nuclear receptor CAR mediates specific xenobiotic induction of drug metabolism. Nature *407*, 920–923.

Yuan, X., Ta, T.C., Lin, M., Evans, J.R., Dong, Y., Bolotin, E., Sherman, M.A., Forman, B.M., and Sladek, F.M. (2009). Identification of an endogenous ligand bound to a native orphan nuclear receptor. PLoS One *4*, e5609.

Zhan, L., Liu, H.X., Fang, Y., Kong, B., He, Y., Zhong, X.B., Fang, J., Wan, Y.J., and Guo, G.L. (2014). Genome-wide binding and transcriptome analysis of human farnesoid X receptor in primary human hepatocytes. PLoS One *9*, e105930.

ISCI, Volume *9*

Supplemental Information

Binding of Drug-Activated CAR/Nr1i3 Alters Metabolic Regulation in the Liver

Jianmin Tian, Rebecca Marino, Carla Johnson, and Joseph Locker

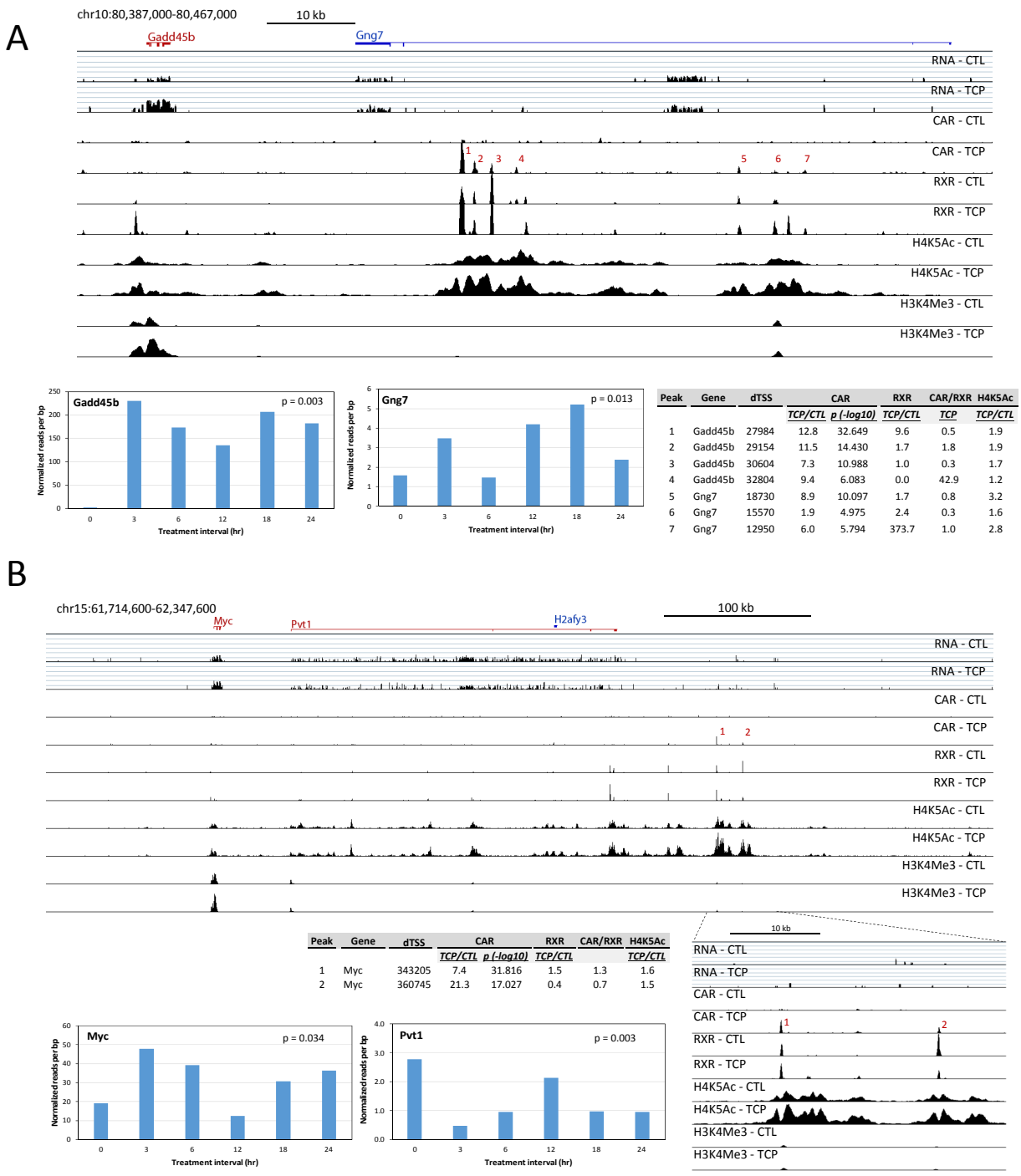

Peak	Gene	dTSS	CAR		RXR	CAR/RXR	H4K5Ac
			TCP/CTL	*p (-log10)*	*TCP/CTL*	*TCP*	*TCP/CTL*
1	Gadd45b	27984	12.8	32.649	9.6	0.5	1.9
2	Gadd45b	29154	11.5	14.430	1.7	1.8	1.9
3	Gadd45b	30604	7.3	10.988	1.0	0.3	1.7
4	Gadd45b	32804	9.4	6.083	0.0	42.9	1.2
5	Gng7	18730	8.9	10.097	1.7	0.8	3.2
6	Gng7	15570	1.9	4.975	2.4	0.3	1.6
7	Gng7	12950	6.0	5.794	373.7	1.0	2.8

Peak	Gene	dTSS	CAR		RXR	CAR/RXR	H4K5Ac
			TCP/CTL	*p (-log10)*	*TCP/CTL*		*TCP/CTL*
1	Myc	343205	7.4	31.816	1.5	1.3	1.6
2	Myc	360745	21.3	17.027	0.4	0.7	1.5

Figure S1. Distant CAR binding associated with two candidate target genes

(A) *Gadd45b* and adjacent *Gng7*. *Gadd45b* is one of the genes most strongly induced by TCPOBOP The region with the closest CAR peaks is within the adjacent gene, *Gng7*.

(B) *Myc* and adjacent *Pvt1*. Among candidate genes stimulated more than 2-fold by TCPOBOP, *Myc* had the most distant linked CAR binding enhancers. Nevertheless, these enhancers were found in a region where even more distant *Myc* enhancers are known. RNA-seq is displayed with $\log_{10}$ and ChIP-seq with linear scales, using GenPlay. Table values are described in Figure 1. Transcript quantifications by RNA-seq were normalized to the values of untreated liver. p values for the time series were calculated by comparison to *Ppia* mRNA (see Table S3).

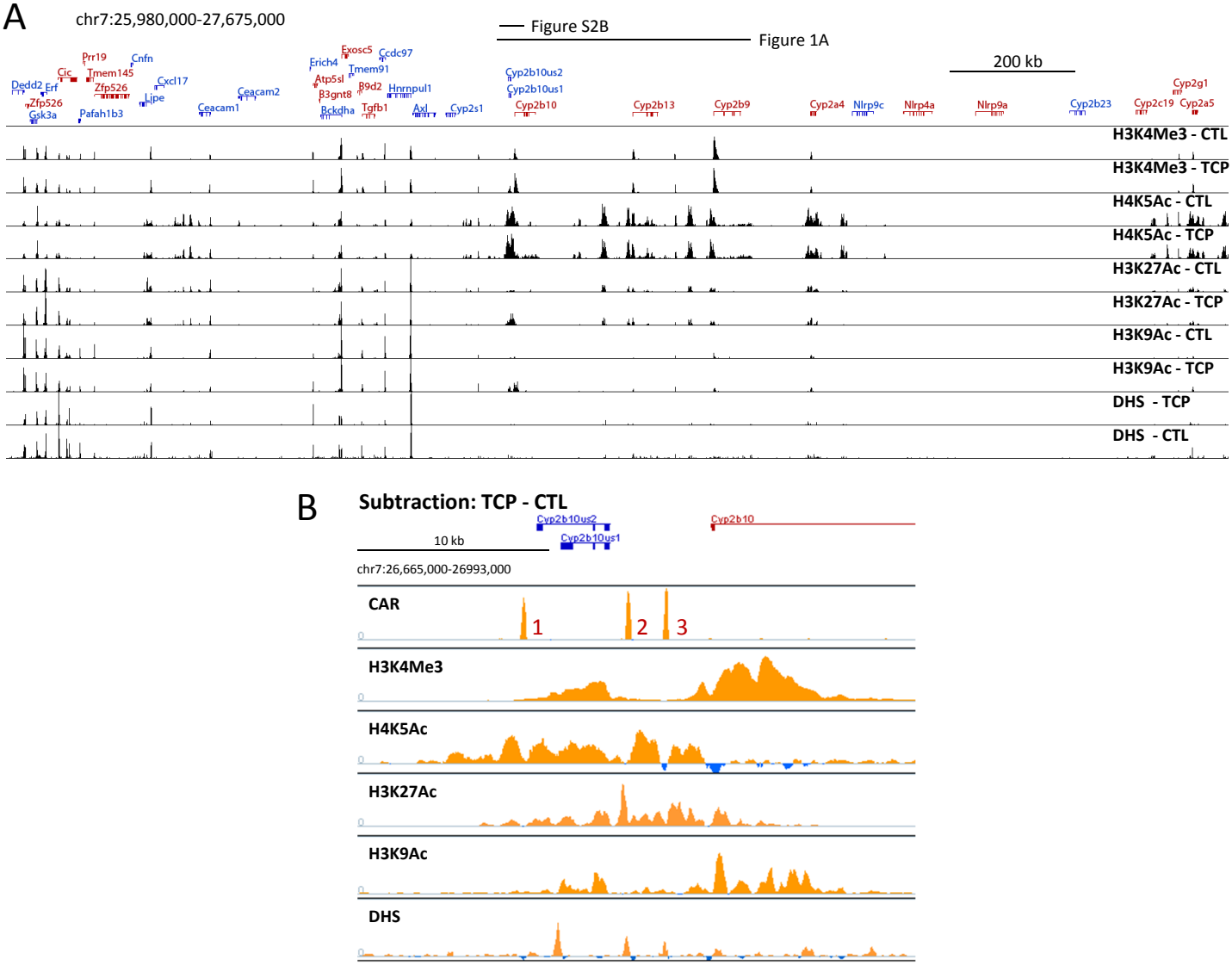

Figure S2. Comparison of chromatin markers in a 1.7 mb region around *Cyp2b10.*
GenPlay visualizations compare promoter-specific H3K4Me3 with acetylated histones H3K9Ac, H3K27Ac, and H4K5Ac, and DNaseI hypersensitivity (DHS), 4 markers that characterize both promoters and enhancers.

A. Overview of a 1.7 Mb region of chromosome 7. The *Cyp2b10-Cyp2b13-Cyp2b9* region displayed in Figure 1A is marked. Note that genes in this region have active promoters with discrete H3K4Me3 peaks, also marked by DHS and the 3 acetylations. The acetylations also mark broader enhancer regions. H4K5Ac provides the strongest detection of enhancer regions and the weakest detection of promoter regions. DHS is a much weaker marker of these enhancer regions. All markers are absent from a distal region of unexpressed genes *(Nlrp4a, Nlrp9a, Cyp2b23*). For comparison, a prox-imal region containing mostly housekeeping genes (e.g., *Hnrnpul1, Ccdc97, Bckdha*) shows strong DHS and acetylation peaks overlying the H3K4Me3-positive promoter peaks. The patterns in this region show that the overall DHS analysis was sensitive despite its weak localization to enhancer regions.

B. Expanded view of the region containing 3 CAR-binding enhancers near *Cyp2b10.* The tracks show the differences calculated by subtracting control from TCPOBOP-treated levels and were amplified to optimally display the subtracted differences. The tracks in panel A more accurately reflect the relative detection sensitivity of H4K5Ac, H3K27Ac, H3K9Ac, and DHS. Note that only H4K5Ac shows strong differences associated with induced CAR peak 1. TCP, TCPOBOP treatment for 3 hr; CTL, untreated control.

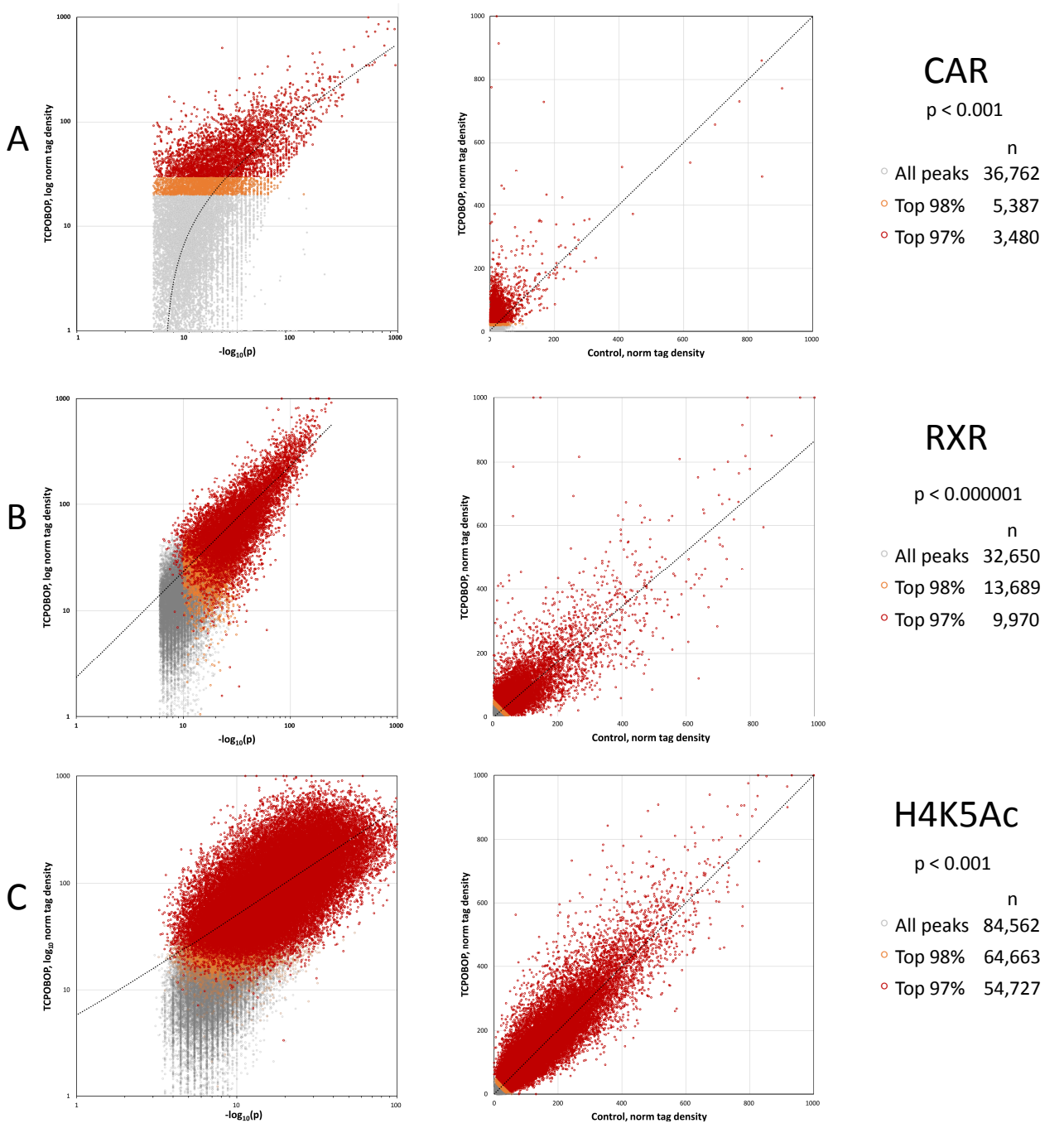

Figure S3. Restriction of CAR, RXR, and H4K5Ac peak sets

(A) CAR. CAR ChIP-seq libraries were compiled with MACS2 and restricted by p-value cutoff (left). However, the majority of significant sites had weak binding so general analysis was further restricted to the top 97% of the range of binding strength (right).

(B) RXR. An RXR peak set was restricted as in panel A.

(C) H4K5Ac. A peak set was compiled using the MACS2 narrow peaks algorithm and restricted as in A. These peaks comprise subregions of fields of H4K5Ac so that 2 adjacent peaks roughly correspond to single enhancers between them.

In all plots, CAR and RXR tag pileups were quantified and normalized to the strongest peak, defined as 1000. Tag density vs p is shown in a log plots, and tag density of control vs treated peaks linear plots.

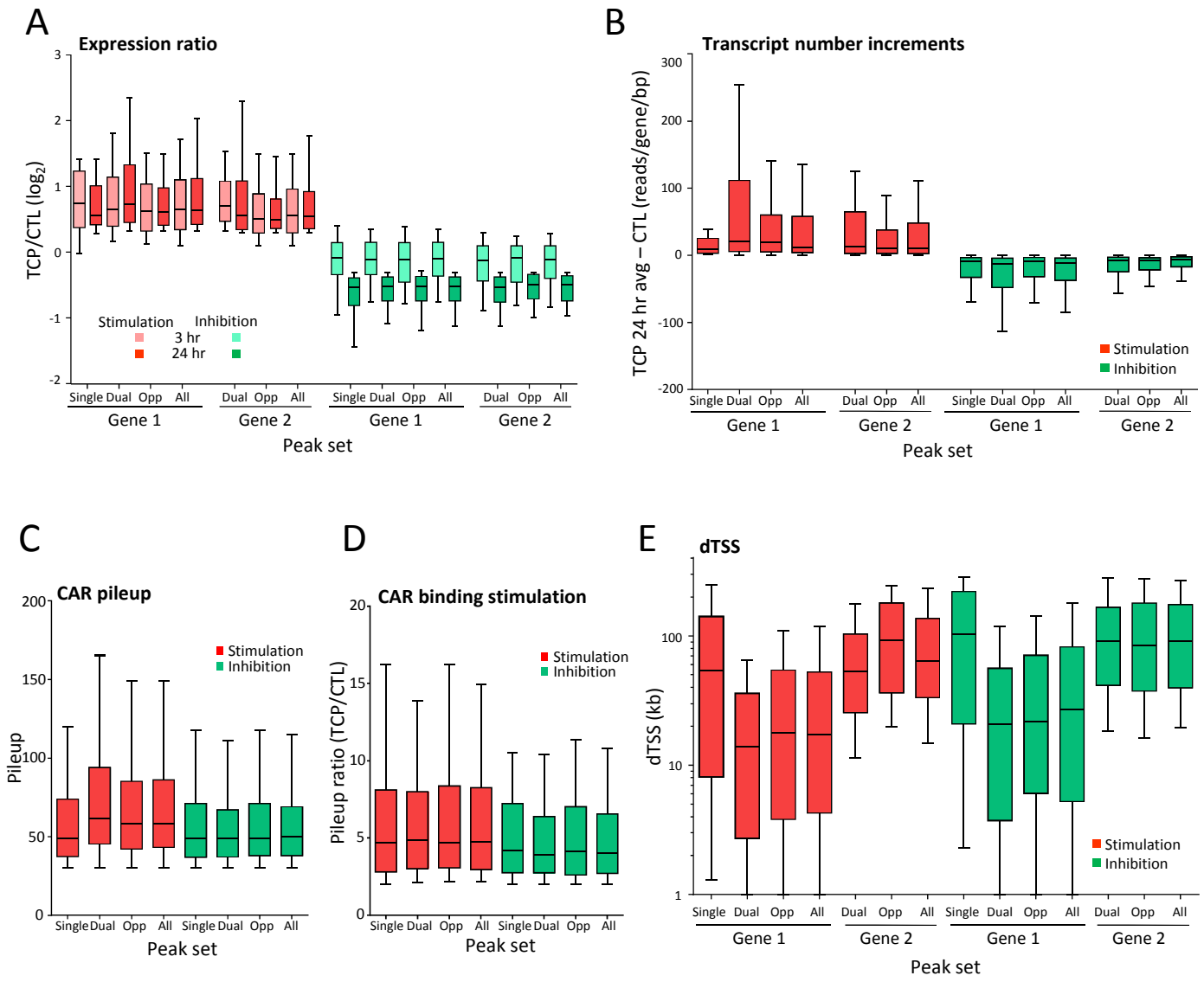

Figure S4. Comparison of peak subsets and linked gene expression

(A) Expression ratios of CAR-linked genes. Subset genes showed comparable stimulation or inhibition. 3 hr and 24 hr avg upregulation were similar, but downregulation was greater in the 24 hr avg.

(B) Transcript number increments. Distributions of incremental change were generally similar, except that Single up genes and more distant genes in dual regulation showed weaker effects.

(C) Pileup and (D) stimulation of CAR binding. Medians of *Single up*, and all peaks linked to down-regulation, were 10 – 15% less than those linked to upregulation.

(E) Distributions of CAR peak-promoter distances. The medians suggest preferred positions for peak-promoter distances: Gene 1, 17 kb and Gene 2, 64 kb for upregulation; 27 kb and 97 kb for downregulation. Peaks associated with single genes correspond to the positions for Gene 2 in the dual sets.

Tukey box plots; Genes 1 and 2, the closer and more distant in each pair, respectively; Subsets: Single, 1 gene/peak; Dual, 2 genes/peak; Opp, paired genes with opposite regulation

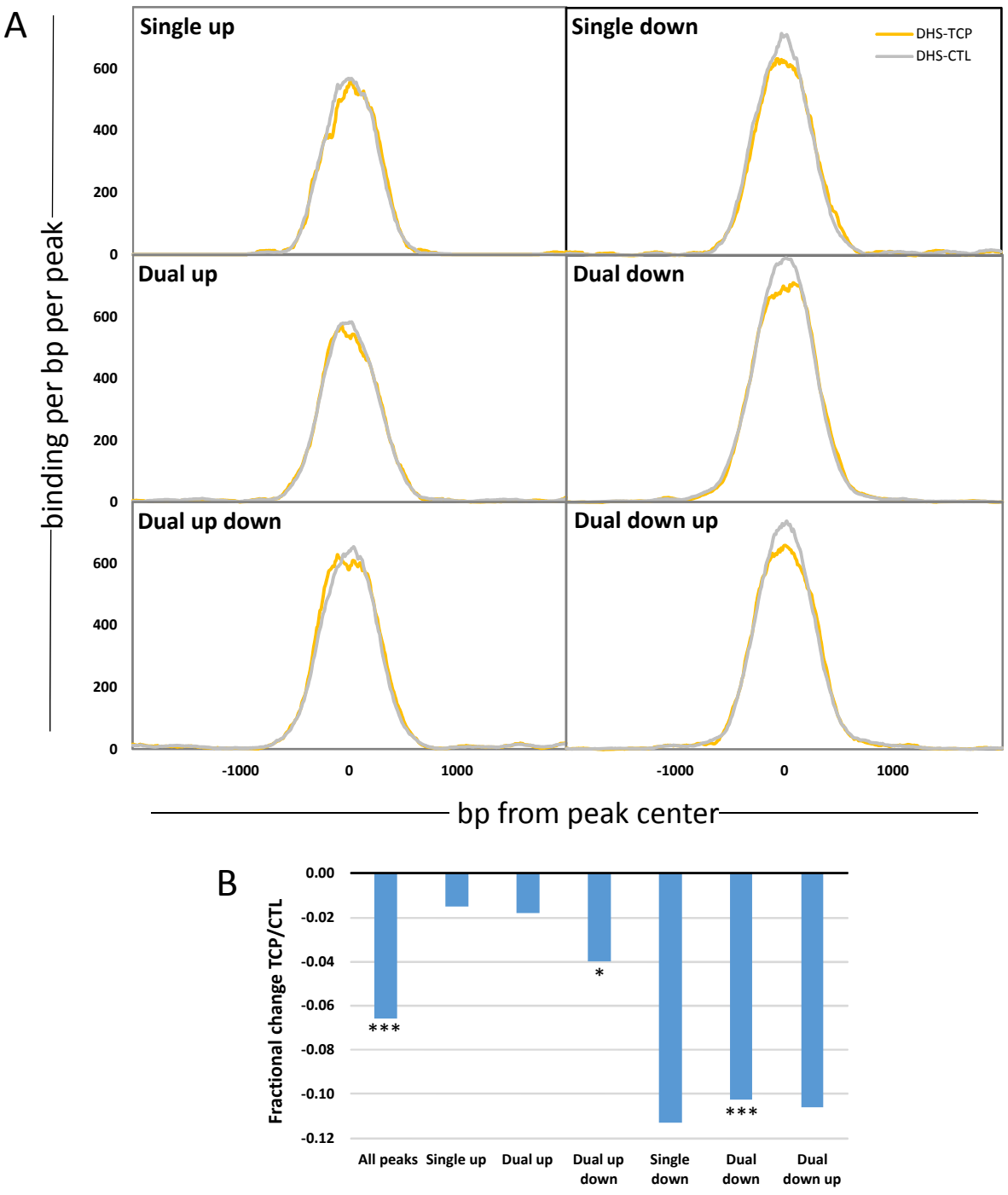

Figure S5. Analysis of DHS in peak-gene subsets

(A) Histogram analysis. Although hypersensitivity is apparent over CAR peaks, TCPOBOP treatment induced focal changes and a small decrease in DHS, particularly in association with downregulation. The changes suggest altered central binding rather than broader chromatin remodeling.

(B) Fractional change of subset DHS levels. The increments represent the fractional difference in DHS reads in a 100-bp window around the CAR peak summits. The DHS reads for individual CAR peaks before and after treatment were compared using paired T-tests. *, $p<0.05$, ***, $p<0.001$.

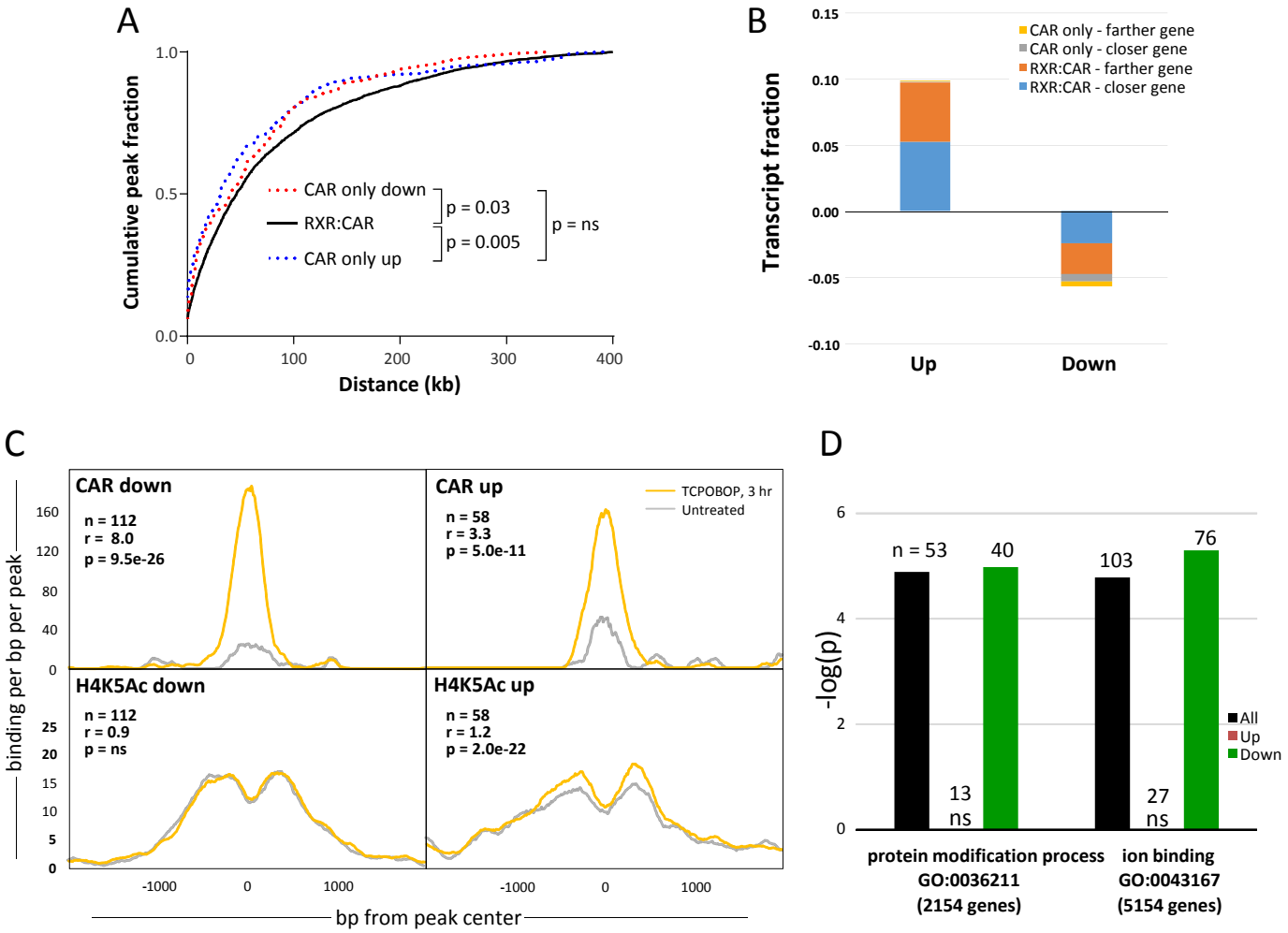

Figure S6. Regulation of gene expression by CAR-only sites

(A) Comparison of TSS distance for CAR-only and RXR:CAR peaks. The CAR-only peaks are moderately closer to promoters.

(B) Transcriptional contribution of unambiguous CAR-only regulation. The CAR-only analysis used peaks associated with genes that were not linked to RXR:CAR sites, 112 down and 58 upregulated genes. The plot shows relative transcription of the two closest genes to each CAR peak and demonstrates that CAR-only-linked transcription is a minor response, predominantly downregulation.

(C) Histogram analysis of CAR binding and H4K5Ac at CAR-only sites. The sites showed the expected binding of CAR. Upregulation was associated with increased H4K5Ac, which was not affected by downregulation, equivalent to correlations observed for RXR:CAR sites.

(D) Ontology profiles of genes regulated by CAR-only sites. The plots show significant correlations to two profiles, entirely through downregulation.

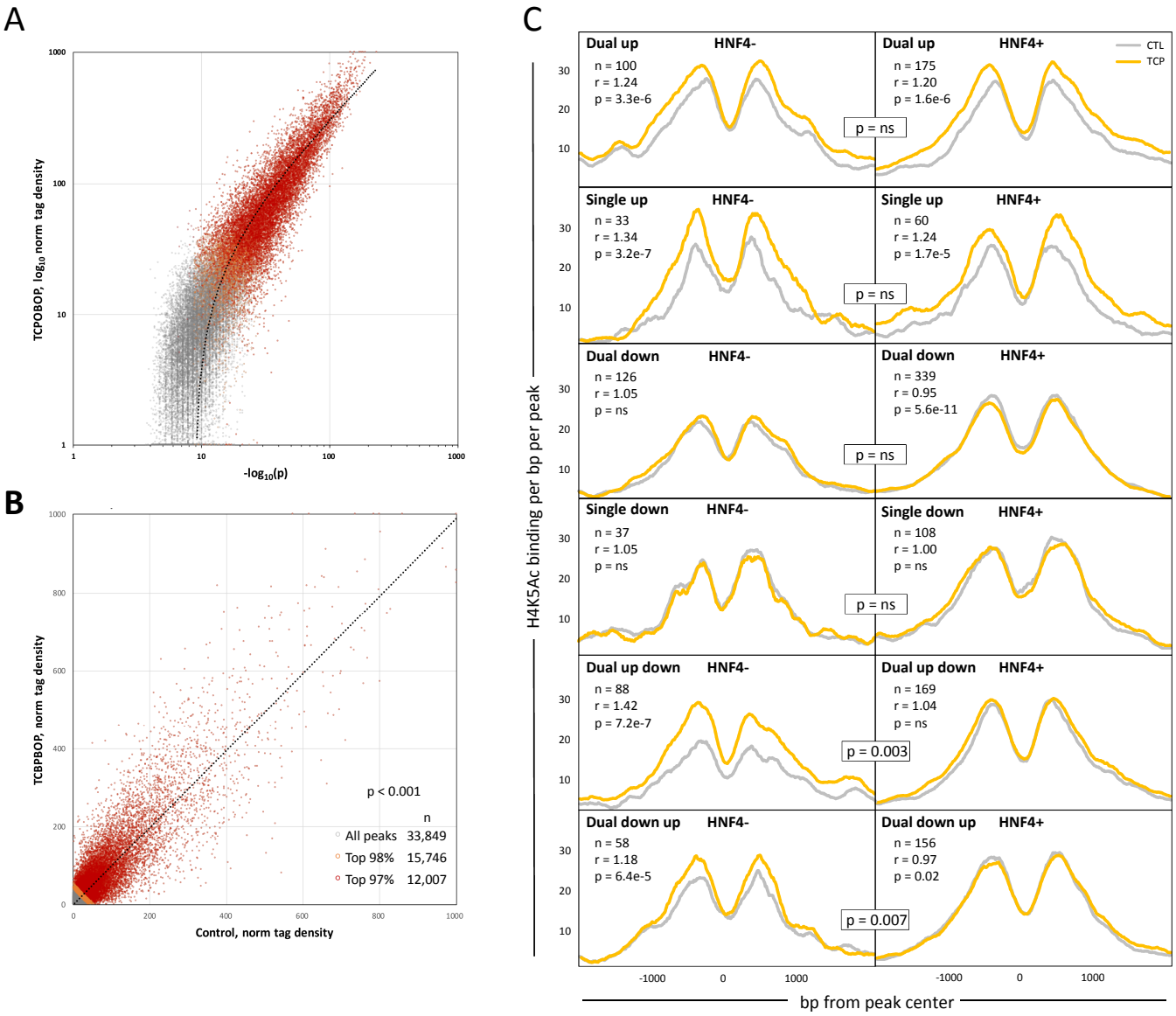

Figure S7. HNF4 analysis

(A) Peak set analysis. A MACS2 peak set was calculated from 4 HNF4α libraries. Treated and control Tag values were then quantified separately. Tag pileups under the calculated peaks were quantified and normalized to the strongest peak, defined as 1000.

(B) Peak set restriction. A linear plot compares pileups from the two experimental conditions. Cutoffs were calculated from the average of Control and TCPOBOP-treated libraries.

(C) Effects of HNF4α on induced H4K5Ac in peak subsets. The 6 CAR peak-gene subsets were divided into HNF4+ and HNF4- groups to compare levels of H4K5Ac before and after TCPOBOP treatment. HNF4 had a highly significant effect, but only in dual opposite peak sets. n, number of peaks in the subset group; r, ratios calculated from treated and untreated peak summits; p, p values calculated using paired T-tests of individual peak values. Boxed p values compare HNF4- and HNF4+ sets, using unpaired T-tests of the stimulation ratios of individual peaks.

TRANSPARENT METHODS

Animals

8-12 week female CD-1 mice (Charles River Laboratories, Wilmington, MA) were treated with TCPOBOP (Millipore Sigma, St. Louis, MO) 3 μg/g body weight in corn oil by gavage. The studies were confined to female mice for uniformity because there is moderate sexual dimorphism. Our prior research focused on females because they develop stronger proliferative responses to this treatment. All animal studies were conducted under protocols approved by the Institutional Animal Care and Use Committees of the University of Pittsburgh in accordance with National Institutes of Health guidelines.

ChIP-seq

Chromatin preparation and immunoprecipitation were carried out as previously described (Tian et al., 2011) with modifications. 3 hr after TCPOBOP treatment, mice were euthanized with inhaled isoflurane and livers rapidly dissected, minced, and treated with 1% formaldehyde in PBS for 10 min at room temperature. After neutralization with 0.125 M glycine for 5 min, liver cells were harvested and washed twice with cold PBS. The liver cell pellet was resuspended in 5 ml/0.5 g liver Cell Lysis Buffer (5 mM PIPES, pH 8.0, 85 mM KCl, 0.5% NP-40). Nuclei were liberated using a B Dounce homogenizer. The number of strokes was determined by microscopic visualization of small aliquots. For lysis, nuclear pellets were suspended in 2 ml/0.5 g liver Nuclear Lysis Buffer (50 mM Tris pH 8.1, 10 mM EDTA, 1% SDS) and incubated on ice for 20 min before sonication.

Nuclei were sonicated with a Diagenode Bioruptor at 4^0 C, using the high setting and 30 sec on/ 30 sec off cycling totaling 20-30 min to produce DNA fragments of 200-500 bp. Fragment size was verified by gel electrophoresis of DNA extracted from aliquots. All buffers were supplemented with Halt protease and phosphatase inhibitors (ThermoFisher).

Immunoprecipitation was carried out with the ChIP-IT high sensitivity kit (Active Motif) using chromatin derived from 15 mg liver and 5 μg antibody for all studies except CAR, which used 25 μg, for each IP. Decrosslinked ChIP DNA was processed with the Illumina TruSeq Nano DNA LT Sample Prep Kit for multiplex sequencing. Individual libraries ranged from 7 – 23 X 10^6 reads. All ChIP-seq analyses combined multiple libraries for each experimental condition. Immunoprecipitations used the following antibodies. Anti-CAR1/2, sc-13065x; RRID:AB_2155209; anti-RXRα, sc-774x; RRID:AB_2270041, and anti-HNF-4 alpha, sc-8987x; RRID:AB_2116913 were obtained from Santa Cruz Biotechnology (Dallas, TX). anti-Histone H4K5ac, 39170; Rabbit anti-Histone H3K4me3, #39915; anti-Histone H3K9Ac, #39137; and anti-Histone H3K27Ac, #39133 were from Active Motif (Carlsbad, CA).

ChIP-seq study of CAR was limited by the availability of suitable antibodies. We previously characterized a series of CAR antibodies and found only one that worked for conventional ChIP (Tian et al., 2011). However, the antibody had blocking activity in gel shift assays, suggesting that the main epitope was within the DNA binding domain and thus inaccessible when CAR was crosslinked to chromatin. Presumably, the ChIP pulldown resulted from a minor epitope. ChIP-seq detection was optimized by titrating antibody concentration to the maximum level that increased peak detection over background. Data was then pooled from libraries of 7 independent livers to further increase sensitivity. Parallel analysis of control liver, which showed few CAR peaks, combined 4 libraries.

RNA-seq and real time PCR
Total liver RNA was prepared with the miRNeasy Mini Kit (Qiagen) and ribosomal RNAs were depleted with the Ribominus Eukaryote System (Life Technology) according to the manufacturer's protocols.

Randomly primed first strand cDNA was synthesized with Superscript III first-strand Synthesis System, (Invitrogen) and real time PCR carried out with Absolute QPCR mix (Fisher). For RNA-seq, second strand cDNA was synthesized with the Superscript Double-Stranded cDNA Synthesis Kit (Fisher).

Double stranded cDNA was then sonicated with the Diagenode Bioruptor at 4^0 C, at low setting and 30 sec on 30 sec off cycling for 30 min, to produce DNA fragments of 150-800 bp. The cDNA was further processed with a TruSeq Nano DNA LT Kit for sequencing. The starting amount of total RNA for each RNA-seq library was 0.75 μg.

PCR primers:
Cyp2b10, 5'-TCTGCTCCATTGTGTTTGGA, 5'-GGCTGGAGAATGAGCTTATGA
Cyp2b10us1, 5'-GGCTCCAGCCCTAGAGACCTACCAG, 5'-CGTGAAAGACACCAACCTGCACA
Cyp2b10us2, 5'-GGCTCCAGCCCTAGAGACCTACCAG, 5'-CGTGAAAGACACCAACCTGCACA
Cyp2b13, 5'-GATCCAACCTTTTTCTTCCAGTGTGTT, 5'-ATTCAGCAAACGCAGGAACTGTTCA
Cyp2b9, 5'-CAGTGCTCCACGAGACTACATTGATACC, 5'-CTCCATAGTGGAGGGTGGCGCTTG

DNase-seq
DNase-seq was modified from a published study (Grontved et al., 2012). Nuclei were isolated from fresh mouse liver as for ChIP experiments, homogenized with a size B Dounce in 30 volumes of DNase I digestion buffer (0.5 M sucrose, 10 mM Tris–HCl, pH 7.5, mM $MgCl_2$, 0.5 mM spermidine, 0.15 mM spermine), and digested with DNase I (Sigma) at 7 Kunitz units per 100 μl for 10 minutes at 30° C. 100-500 bp DNA fragments were purified from an Invitrogen 2% E-Gel 2% and further prepared as for ChIP-seq.

Sequencing and data analysis
Enriched DNA from ChIP-seq and DNase-seq libraries were analyzed with 50 bp single end, RNA-seq with 100 bp paired end, reads on an Illumina Hiseq 2500 at the Epigenetics Shared Facility of Albert Einstein College of Medicine in New York. Sequences were aligned to the mm9 reference genome through the bioinformatic pipeline at the same facility. For RNA-seq, transcript quantification, statistical testing, and annotation were performed using Cufflinks (Trapnell et al., 2012) or GenPlay (Lajugie and Bouhassira, 2011) programs.

Filtering of non-analyzable genomic regions
Initial ChIP-seq studies compared treated liver to control immunoprecipitations with normal serum. In the compiled sets, thousands of peaks were stronger than those associated with the most stimulated candidate genes. Visualization showed these strong peaks clustered to a few regions and were present in both CAR and normal-serum libraries. The latter, however, did not contain enough information to filter them. We therefore computationally enlarged the peak regions using GenPlay until they coalesced into regions and then visually adjusted their boundaries. The

nonanalyzable regions were compiled in a BED file as an mm9 artifact filter (Table S1). For ChIP-seq and DNase-seq, these regions were filtered from individual BAM files using BEDtools (Quinlan and Hall, 2010). The analysis also excluded chrY, chrM, and random unassembled genome segments.

Compilation and analysis of ChIP-seq peak sets

After filtering the BAM files, peak sets were generated using MACS2 (Feng et al., 2012). For CAR analysis, 7 treated libraries were combined to define peaks. For other NR, chromatin modifications, and DNAse-seq, treated and untreated libraries were first combined together to define a peak set. Treated and untreated libraries were then combined separately with MACS2 and pileups quantified from each in GenPlay using the defined peak set.

Restriction of peak sets used only unbiased criteria: p-value and fraction of the total range of pileup values, usually excluding the bottom 3%. CAR analysis used an additional criterion, stimulation ratio, to exclude a few hundred peaks. MEME-ChIP analysis was used to validate the ratio cutoff, via detection of the RXR half site motif (Figure 2E), which was present in some peaks with a stimulation ratio < 1.7, but none with a ratio <1.5.

Downstream analysis was carried out using BEDtools, the HOMER suite (Heinz et al., 2010), RnaChipIntegrator (https://github.com/fls-bioinformatics-core/RnaChipIntegrator), and the MEME suite (Bailey et al., 2015). In particular, generation of tag directories, histogram analysis, and Functional Enrichment Analysis used HOMER programs. De novo motif discovery used MEME-ChIP and subsequent scanning of these motifs used FIMO. For motif localization, random control sets were generated by the BEDtools program, Shuffle, matched by chromosome location, and length. Overlap of peaks was calculated using the BEDtools Intersect default setting (1-base overlap). For H4K5Ac, this method of overlap calculation was applied only to the data in Figure 2C. Subsequent analysis used HOMER calculations of H4K5Ac tag density within a 1000-bp window around CAR peaks.

Quantification of the hepatocyte transcriptome

The hepatocyte transcriptome was compiled from 9 RNA-seq libraries: 2 controls, 2 each after TCPOBOP treatment of 3 and 6 hr, and 1 each from treatments of 12, 18, and 24 hr. The libraries were quantified with GenPlay as raw exon reads that aligned with the Refseq annotation of 30,255 genes in the mm9 genome. Values and annotations for rRNA, mtRNA, and genes shorter than 130 bp were removed. The analysis also excluded chrY and random unassembled genome segments. Isoforms with duplicate gene names were also removed, retaining the isoform with the greatest number of reads. Of the resultant list of 24,000 unique annotations, 16,800 genes had measurable expression. Libraries then received simple linear normalization using the total number of reads. These values reflect transcript mass (as reads/transcript). Following normalization, the values were divided by molecular weight to reflect transcript number (as reads/kb/transcript).

For individual time points, expression was compared as ratios to control reads. A second parameter, average hourly expression over 24 hr (24 hr avg reads), was calculated from the whole set of libraries to provide a single parameter that represented the full time course ($(3 \times (r_0 + r_3)/2 + 3 \times (r_3 + r_6)/2 + 6 \times (r_6 + r_{12})/2 + 6 \times (r_{12} + r_{18})/2 + 6 \times (r_{18} + r_{24})/2) / 24$); r, reads; subscripts, hr after treatment.

For statistical analysis, the series of expression ratios for each transcript (t = 0, 3, 6, 12, 18, and 24) was compared to Ppia mRNA using one-tailed paired T tests and was further refined by calculation of Benjamini-Hochberg FDR.

The data were also compared to 2 libraries from isolated control hepatocytes to filter out non-hepatocyte transcripts, defined as >80% depletion compared to whole liver. The hepatocyte transcriptome of 12,440 genes encompassed a 5-log range of expression. mRNA number was calculated from the reads per gene of the most abundant transcript, *Alb,* ~20,000 molecules/cell. Expression levels at the low end of the transcriptome represented approximately 0.1 transcripts per cell.

Data and Software Availability

Raw datasets were deposited in the NCBI SRA database: RNA-seq, SRP125909; ChIP-seq and DNAse-seq, SRP125957. Raw datasets were deposited in the NCBI SRA database: RNA-seq, SRP125909; ChIP-seq and DNAse-seq, SRP125957.

ChIP-seq and DNAse-seq FASTQ libraries

acc	name	organism	tag	value
SRS2727669	ChIPseq-CAR-CTL-rep-1	Mus musculus	strain	CD1
SRS2727668	ChIPseq-CAR-CTL-rep-2	Mus musculus	strain	CD1
SRS2727666	ChIPseq-CAR-CTL-rep-3	Mus musculus	strain	CD1
SRS2727667	ChIPseq-CAR-CTL-rep-4	Mus musculus	strain	CD1
SRS2727665	ChIPseq-CAR-TCP-rep-1	Mus musculus	strain	CD1
SRS2727664	ChIPseq-CAR-TCP-rep-2	Mus musculus	strain	CD1
SRS2727662	ChIPseq-CAR-TCP-rep-3	Mus musculus	strain	CD1
SRS2727663	ChIPseq-CAR-TCP-rep-4	Mus musculus	strain	CD1
SRS2727670	ChIPseq-CAR-TCP-rep-5	Mus musculus	strain	CD1
SRS2727671	ChIPseq-CAR-TCP-rep-6	Mus musculus	strain	CD1
SRS2727688	ChIPseq-CAR-TCP-rep-7	Mus musculus	strain	CD1
SRS2727689	ChIPseq-RXRa-CTL-rep-1	Mus musculus	strain	CD1
SRS2727690	ChIPseq-RXRa-CTL-rep-2	Mus musculus	strain	CD1
SRS2727691	ChIPseq-RXRa-TCP-rep-1	Mus musculus	strain	CD1
SRS2727684	ChIPseq-RXRa-TCP-rep-2	Mus musculus	strain	CD1
SRS2727685	ChIPseq-RXRa-TCP-rep-3	Mus musculus	strain	CD1
SRS2727686	ChIPseq-RXRa-TCP-rep-4	Mus musculus	strain	CD1
SRS2727687	ChIPseq-HNF4a-CTL-rep-1	Mus musculus	strain	CD1
SRS2727681	ChIPseq-HNF4a-CTL-rep-2	Mus musculus	strain	CD1
SRS2727682	ChIPseq-HNF4a-TCP-rep-1	Mus musculus	strain	CD1
SRS2727677	ChIPseq-HNF4a-TCP-rep-2	Mus musculus	strain	CD1
SRS2727672	ChIPseq-H3K4me3-CTL-rep-1	Mus musculus	strain	CD1
SRS2727675	ChIPseq-H3K4me3-CTL-rep-2	Mus musculus	strain	CD1
SRS2727674	ChIPseq-H3K4me3-TCP-rep-1	Mus musculus	strain	CD1
SRS2727683	ChIPseq-H3K4me3-TCP-rep-2	Mus musculus	strain	CD1
SRS2727676	ChIPseq-H4K5Ac-CTL-rep-1	Mus musculus	strain	CD1
SRS2727679	ChIPseq-H4K5Ac-CTL-rep-2	Mus musculus	strain	CD1
SRS2727678	ChIPseq-H4K5Ac-TCP-rep-1	Mus musculus	strain	CD1

SRS2727673	ChIPseq-H4K5Ac-TCP-rep-2	Mus musculus	strain	CD1
SRS2727680	ChIPseq-H3K9Ac-CTL	Mus musculus	strain	CD1
SRS2727696	ChIPseq-H3K9Ac-TCP	Mus musculus	strain	CD1
SRS3489116	ChIP-seq-H3K27-CTL	Mus musculus	strain	CD1
SRS3489115	ChIP-seq-H3K27-TCP	Mus musculus	strain	CD1
SRS2727697	Dnaseseq-CTL-rep-1	Mus musculus	strain	CD1
SRS2727693	Dnaseseq-CTL-rep-2	Mus musculus	strain	CD1
SRS2727695	Dnaseseq-TCP-rep-1	Mus musculus	strain	CD1
SRS2727694	Dnaseseq-TCP-rep-2	Mus musculus	strain	CD1
SRS2727692	Dnaseseq-TCP-rep-3	Mus musculus	strain	CD1

RNA-seq FASTQ libraries

acc	name	organism	tag	value
SRS2725635	RNA-seq-ctrl-rep-1	Mus musculus	strain	CD1
SRS2725634	RNA-seq-ctrl-rep-2	Mus musculus	strain	CD1
SRS2725633	RNA-seq-TCP-3h-rep-1	Mus musculus	strain	CD1
SRS2725632	RNA-seq-TCP-3h-rep-2	Mus musculus	strain	CD1
SRS2725639	RNA-seq-TCP-6h-rep-1	Mus musculus	strain	CD1
SRS2725638	RNA-seq-TCP-6h-rep-2	Mus musculus	strain	CD1
SRS2725637	RNA-seq-TCP-12h	Mus musculus	strain	CD1
SRS2725636	RNA-seq-TCP-18h	Mus musculus	strain	CD1
SRS2725631	RNA-seq-TCP-24h	Mus musculus	strain	CD1
SRS2725640	CD1-Hepatocyte	Mus musculus	strain	CD1
SRS3489136	CD1-Hepatocyte-rep-2	Mus musculus	strain	CD1

Published datasets analyzed in this study

PPARα, ChIP-seq (GSE35262), expression (GSE8295); FXR, ChIP-seq (downloaded from the UCSC data base with the link from (Thomas et al., 2010)), expression (GSE57305); LXRα, ChIP-seq (GSE35262), expression (Boergesen et al., 2012); PXR, ChIP-seq (kindly provided by Dr. J. Cui, University of Washington), expression (GSE55746); THR, ChIP-seq (SRX879758), expression (GSE65947)

Supplementary References

Bailey, T.L., Johnson, J., Grant, C.E., and Noble, W.S. (2015). The MEME Suite. Nucleic Acids Res *43*, W39-49.

Boergesen, M., Pedersen, T.A., Gross, B., van Heeringen, S.J., Hagenbeek, D., Bindesboll, C., Caron, S., Lalloyer, F., Steffensen, K.R., Nebb, H.I., et al. (2012). Genome-wide profiling of liver X receptor, retinoid X receptor, and peroxisome proliferator-activated receptor alpha in mouse liver reveals extensive sharing of binding sites. Mol Cell Biol *32*, 852-867.

Feng, J., Liu, T., Qin, B., Zhang, Y., and Liu, X.S. (2012). Identifying ChIP-seq enrichment using MACS. Nat Protoc *7*, 1728-1740.

Grontved, L., Bandle, R., John, S., Baek, S., Chung, H.J., Liu, Y., Aguilera, G., Oberholtzer, C., Hager, G.L., and Levens, D. (2012). Rapid genome-scale mapping of chromatin accessibility in tissue. Epigenetics Chromatin *5*, 10.

Heinz, S., Benner, C., Spann, N., Bertolino, E., Lin, Y.C., Laslo, P., Cheng, J.X., Murre, C., Singh, H., and Glass, C.K. (2010). Simple combinations of lineage-determining transcription factors prime cis-regulatory elements required for macrophage and B cell identities. Mol Cell *38*, 576-589.

Lajugie, J., and Bouhassira, E.E. (2011). GenPlay, a multipurpose genome analyzer and browser. Bioinformatics *27*, 1889-1893.

Quinlan, A.R., and Hall, I.M. (2010). BEDTools: a flexible suite of utilities for comparing genomic features. Bioinformatics *26*, 841-842.

Tian, J., Huang, H., Hoffman, B., Liebermann, D.A., Ledda-Columbano, G.M., Columbano, A., and Locker, J. (2011). Gadd45beta is an inducible coactivator of transcription that facilitates rapid liver growth in mice. J Clin Invest *121*, 4491-4502.

Trapnell, C., Roberts, A., Goff, L., Pertea, G., Kim, D., Kelley, D.R., Pimentel, H., Salzberg, S.L., Rinn, J.L., and Pachter, L. (2012). Differential gene and transcript expression analysis of RNA-seq experiments with TopHat and Cufflinks. Nat Protoc *7*, 562-578.